J. Fluid Mech. (1994), *vol.* 267, *pp.* 23–51

Multipolar vortices in two-dimensional incompressible flows

By YVES G. MOREL[1] AND XAVIER J. CARTON[2]

[1]SHOM, LEGI/IMG, BP53X, 38041 Grenoble Cedex, France

[2]SHOM, GRGS, Centre National d'Etudes Spatiales, 18 Ave. Edouard Belin, 31055 Toulouse Cedex, France

(Received 9 March 1993 and in revised form 9 November 1993)

In a two-dimensional incompressible fluid, the barotropic instability of isolated circular vortices can lead to multipole formation. The multipoles we study here are composed of a core vortex surrounded by two or more identical satellite vortices, of opposite-sign vorticity to the core, and the total circulation is zero. First, we present the generation of multipoles from unstable piecewise-constant monopoles perturbed on a monochromatic azimuthal mode. The stationary multipoles formed by this nonlinear evolution retain the same energy, circulation and angular momentum as the original monopoles, but possess a lower enstrophy. These multipolar steady states are then compared to multipolar equilibria of the Euler equation, obtained either analytically by a perturbation expansion or numerically via a relaxation algorithm. Finally the stability of these equilibria is studied. Quadrupoles (one core vortex bound to three satellites) prove relatively robust, whether initially perturbed or not, and resist severe permanent deformations (mode-2 shears or strains of amplitude up to $0.1\zeta_{max}$). Amplification of the mode-3 deformation proves more destructive. More complex multipoles degenerate in less than a turnover period into end-products of a lesser complexity, via vortex splitting, pairing or merging. We use the conservation of integral properties to classify the large variety of instability mechanisms along physical guidelines. To conclude, we synthetize the connections between these various vortex forms.

1. Introduction

Coherent vortices are long-lived, horizontally recirculating fluid motions of compact size, which play an essential role in transient flows, such as unstable ocean currents or two-dimensional turbulence (McWilliams 1984, 1990). These vortices are usually circular, isolated, their dynamics is dominated by the Coriolis force, their Rossby number $Ro = U/fL$ is small and their velocity field is horizontal and non-divergent at zeroth order in Ro. In the ocean, such 'mesoscale' structures are noticeable both in size and life-span (50–200 km and a few weeks to a few months); they carry large momentum and specific water masses far away from their region of production, consequently contributing to the energy, heat and tracer budgets. In two-dimensional free-decay turbulence, vortex interactions (merger and pairing) eventually yield isolated circular structures, but also dipolar or tripolar aggregates (Legras, Santangelo & Benzi 1988).

The literature on isolated vortex stability now covers monopoles, dipoles, tripoles,

annuli and vortices on a ring (Gent & McWilliams 1986; Flierl 1988; Carton & McWilliams 1989; Carton, Flierl & Polvani 1989; Bell 1990; Orlandi & van Heijst 1992; Carton & Legras 1994; Pierrehumbert 1980; McWilliams & Zabusky 1982; McWilliams 1983; Polvani & Carton 1990; Kozlov & Makarov 1985; Dritschel 1985, 1986). A natural formation of dipoles and tripoles from unstable monopoles has been confirmed by laboratory experiments (van Heijst & Flor 1989; van Heijst, Kloosterziel & Williams 1989). It has also been shown that more complex vortex structures than tripoles can be formed from strongly perturbed two-dimensional vortices (Carton 1992). Still, the effects of barotropic instability leading to complex vortex aggregates need to be more fully assessed (Hopfinger & van Heijst 1993).

At present, the stability of all regular vorticity distributions with an axial symmetry cannot be determined by means of a general criterion based on a simple physical principle. Variational techniques have provided only two exact analytical vortex solutions of the nonlinear Euler equation: the minimum-enstrophy vortex (Leith 1981) and the variational modons (Stern 1974). In the extreme idealization of point-multipoles, quantitative stability estimates have been obtained which give an upper limit on the number of vortices which can be stably and symmetrically bound (Morikawa & Swenson 1971). Unfortunately, finite-area effects render realistic vortex dynamics somewhat different from the singular point-vortex cases, e.g. by coherent dipole formation, by filamentation or merger (Melander, Zabusky & McWilliams 1988). To efficiently idealize finite-area vortices, we use here the well-known Finite-Area Vorticity Region (FAVR) framework; it represents vortices as piecewise-constant in the midst of an irrotational medium (Deem & Zabusky 1978). This approximation allows a detailed investigation of a dimensionally reduced parameter space, while a good dynamical agreement still exists between continuous vortices and their FAVR counterparts (Legras & Dritschel 1993).

This paper aims at describing the generation, stationary forms and stability of two-dimensional multipolar FAVR's. We first present an efficient mechanism to generate them from barotropically unstable FAVR monopoles. The linear stability of these monopoles is studied analytically and their nonlinear evolution is modelled with a contour surgery and a pseudospectral code (§3). The end-products of this instability are compared to multipolar steady states of the Euler equation, obtained with analytical perturbation expansions or with a numerical algorithm (§4). The stability of these multipolar equilibria is then examined to determine which are naturally stable, or robust when slightly perturbed or permanently deformed (§5). In §6, we show how the conservation of integral properties can help predict the vortex transformations. Finally we summarize the properties and relations of these different vortex types.

2. The barotropic vorticity equation

A reasonable assumption for vortex studies (on Earth or in a spinning water tank) is the dominance of the entrainment rotation over inertial mechanisms which renders flows quasi-two-dimensional. Non-divergence of the horizontal velocity field (which thus derives from a streamfunction ψ) is inserted into Ertel's theorem to yield the barotropic vorticity equation

$$\partial_t \zeta + J(\psi, \zeta) = \nu \nabla^6 \psi, \tag{2.1}$$

where $\zeta = \nabla^2 \psi$ is the vorticity, and ψ the streamfunction. The right-hand term of (2.1) is a numerical artifact known as biharmonic viscosity and is used here only in Eulerian

gridded models. In most cases, the dynamics are purely inviscid ($\nu = 0$). Then if the spatial domain is bounded by a streamline, (2.1) has the following invariants: excess energy (the area integral $-\frac{1}{2}\int \zeta\psi \mathrm{d}A$, here the kinetic energy), angular momentum ($\int r v_\theta \mathrm{d}A$, where v_θ is the azimuthal velocity), circulation, enstrophy and more generally any moment of the vorticity ($\int \zeta^n \mathrm{d}A$, see also Dritschel 1985).

Hereafter, we use two numerical discretizations of the nonlinear form of (2.1): a Lagrangian and an Eulerian model. The Lagrangian model assumes that ζ is strictly piecewise-constant (FAVR hypothesis) and that the domain extends to infinity in both directions; then ψ as a function of ζ reduces to a sum of contour integrals on vortex boundaries (Deem & Zabusky 1978; Dritschel 1985):

$$\vec{u}(x, y) = -\frac{1}{4\pi}\sum_{k=0}^{N+1}\gamma_k \int_{\partial A_k} \log(|\vec{x} - \vec{x}_k|^2)\,\mathrm{d}\vec{x}_k. \tag{2.2}$$

The nodes which produce these boundaries are advected by the total velocity field. This technique is known as contour dynamics and represents the Euler equation ($\nu = 0$ in (2.1)). The density of nodes is a function of the local curvature of the boundary. In the case of intense contour deformations, this number, hence the computational burden, would drastically increase. Therefore, in the presence of long thin filaments or of narrow bridges between vortices, the vorticity patches are disconnected; this occurs when the distance between close nodes drops below a threshold given by a parameter μ. A similar procedure reconnects vortices closer than this critical distance. A parameter $\lambda = \mu^2 L/8$, where L is a prescribed large scale (here unity), controls the number of nodes on each contour; this scheme, known as contour surgery, introduces a very limited form of dissipation (Dritschel 1988). In this code, the vorticity is normalized by a factor 2π, so that a physical timescale based on an eddy turnover period is unity.

The second representation of (2.1) we use is the by-now classic pseudospectral gridded model (see for instance McWilliams 1984, for a description). The domain is periodic in x and y. The resolution is 256 gridpoints in each direction and the box length is 2π. Maximum vorticity is normalized to unity so that an eddy timescale is 2π. The time-step is 0.025 for 256 horizontal nodes (to satisfy the Courant–Friedrich–Lewy stability condition). Hyperviscosity, the right-hand side of (2.1), is used to prevent enstrophy accumulation at small scales though ν is kept minimum, $\nu = 10^{-8}$. Spurious vortex interactions by periodicity are avoided by a small ratio of vortex size to domain length and by a zero total vortex circulation. Vorticity jumps at vortex boundaries, which should generate Gibb's instability, are smoothed by an iterative procedure (Polvani & Carton 1990) or initially defined as exponentially decreasing.

3. Generation of multipoles from unstable circular vortices

A necessary condition for barotropic instability of two-dimensional vortices is the existence of a point of inflexion in their radial vorticity profile (Rayleigh's theorem, 1880). In the case of a FAVR monopole (a piecewise-constant vorticity profile), this condition can be replaced by the existence of two vorticity regions of opposite sign (a.k.a. vorticity shielding). These two regions can be adjacent (see figure 1*a*), a configuration we refer to as a two-contour (Rankine) vortex, or they can be separated by a region of null vorticity, a state which we call three-contour (Rankine) vortex (figure 1*b*).

Two-contour Rankine vortices have been investigated at length recently and exhibit

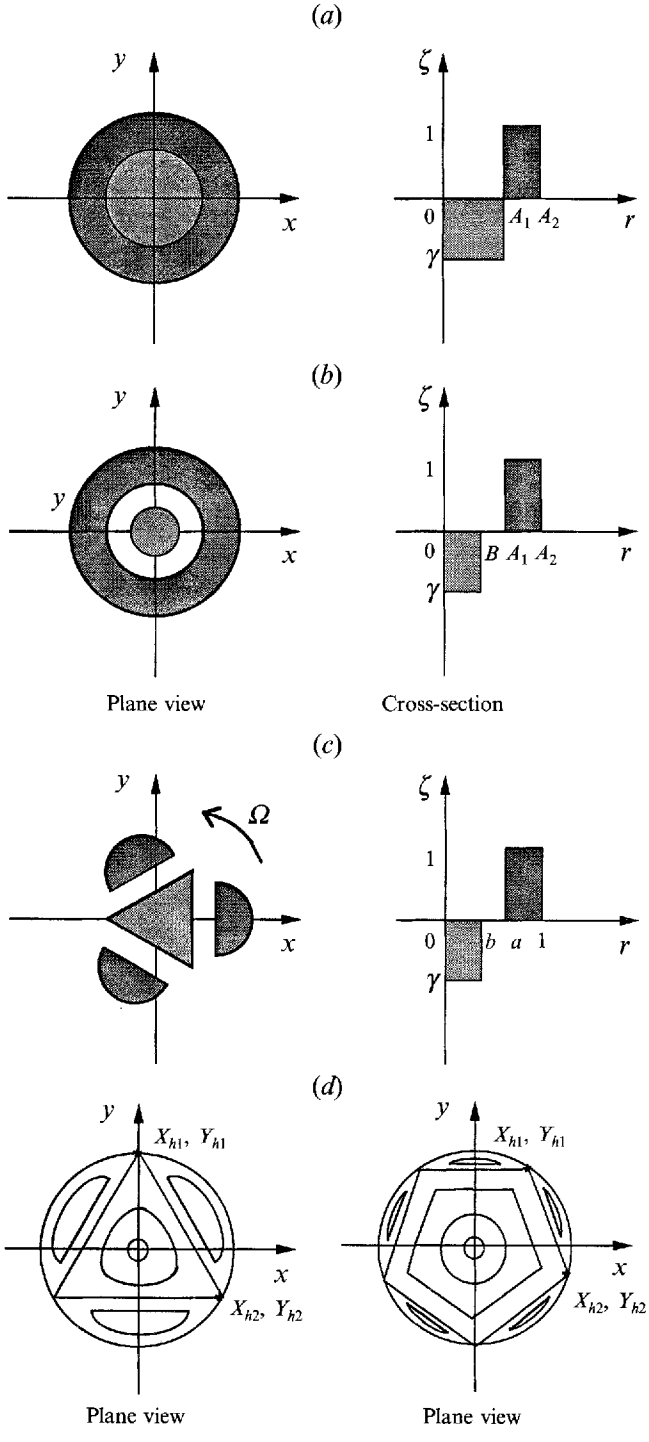

FIGURE 1. Generic design of (*a*) a two-contour and (*b*) a three-contour Rankine vortex, (*c*) a multipole and (*d*) the corotating streamfunction ψ_c of a multipole, for this study.

a natural tendency to break into dipoles when barotropically unstable (see figure 14 of Flierl 1988). Only a few two-contour shielded vortices create a long-lasting quadrupole or a pentapole; this requires that they be strongly perturbed initially (see figure 4 of Carton 1992). From the generic form of a two-contour vortex (figure 1*a*) and that of a multipole (figure 1*c*), we can understand that a major geometrical rearrangement of the vorticity has to take place to transform the former into the latter. Indeed, zero-vorticity fluid initially exterior to the circular vortex has to intrude between the two vorticity regions during this transformation. Moreover, while the outer boundary of the circular vortex has to reconnect into separate satellite boundaries in the multipole, the original inner boundary should remain only slightly deformed in the end. This can be achieved solely if the outer boundary is originally very perturbed.

On the other hand, in the case of a three-contour Rankine vortex, a region of zero-vorticity fluid already exists in the circular vortex between the two finite-vorticity regions. In this case, the outer annulus (of unit vorticity) can reorganize into separate satellites independently of the core transformation. Complex multipoles should thus be formed much more easily. Hereafter, we therefore use such three-contour vortices to generate multipoles.

3.1. *Linear instability of three-contour Rankine vortices*

For consistency with the previous study on tripoles (Polvani & Carton 1990), we choose the following geometrical and physical parameters for the three-contour Rankine vortex (see figure 1*b*):

a central (core) vortex of radius B and vorticity $\gamma < 0$;
an inert (buffer) zone between $r = B$ and $r = A_1$ of zero vorticity;
an annulus between $r = A_1$ and $r = A_2$ of positive unit vorticity.

This choice of mean flow is supported by observations both of atmospheric (Lin 1992) and of oceanic (Dombrowsky, personal communication) vortices. Another example of a three-contour Rankine vortex – shielded annuli with vorticities 0, ω_1, ω_2, 0 from the centre to the periphery – has been studied by Kozlov & Makarov (1985); they showed that the various annuli would split regularly on azimuthal modes 2, 3, and 4 and irregularly for smaller wavelength disturbances. Here, the parameter space is three-dimensional (all lengthscales can be renormalized by A_2) and we present mathematical results for general values of A_1, A_2, B and γ (general cases). Still, only those vortices with zero total circulation have finite energy; we call these the special cases that are studied numerically here. General cases have been studied at length and do not exhibit significant differences with these special cases (e.g. Morel & Carton 1991). The zero-circulation condition is written

$$\Gamma_t = \gamma B^2 + A_2^2 - A_1^2 = 0. \tag{3.1}$$

The velocity field of the three-contour Rankine vortex, hereafter named mean flow, is in the general case

$$\begin{aligned}
&\bar{U}(r) = \gamma r/2, && r \leqslant B && \text{(region 1)};\\
&\bar{U}(r) = \gamma B^2/(2r), && B \leqslant r \leqslant A_1 && \text{(region 2)};\\
&\bar{U}(r) = \gamma B^2/(2r) + r/2 - A_1^2/(2r), && A_1 \leqslant r \leqslant A_2 && \text{(region 3)};\\
&\bar{U}(r) = \Gamma_t/(2r), && A_2 \leqslant r, && \text{(external flow).}
\end{aligned}$$

To analyse the linear stability of this vortex, we linearize (2.1) with $\nu = 0$ to obtain the Rayleigh equation and we assume that the perturbation is a normal mode of the

form

$$\psi'(r,\theta,t) = \phi(r)\,\mathrm{e}^{\mathrm{i}\ell(\theta - ct)}. \tag{3.2}$$

Eventually we have to solve a 3×3 determinant to obtain a third degree equation for $\sigma = 2\ell c$ (see Dritschel 1989):

$$\begin{aligned}
&\sigma^3 + \sigma^2\gamma\,(1 - \ell - \ell\,\beta^2/\alpha^2 - \ell\,\Gamma_t/\gamma) + \sigma\gamma\,[(\ell - 1)(1 + \ell\,\gamma\,\beta^2/\alpha^2) \\
&+ (1 - \ell - \ell\,\beta^2/\alpha^2 - 1/\gamma)(1 - \alpha^{2\ell} - \ell\,\Gamma_t) - \beta^{2\ell} + (\beta/\alpha)^{2\ell} - \alpha^{2\ell}(\ell - 1 + \ell\,\beta^2/\alpha^2)] \\
&+ \gamma\,(1 - \alpha^{2\ell} - \ell\,\Gamma_t)\,[(\beta/\alpha)^{2\ell} + (\ell - 1)(1 + \ell\,\gamma\beta^2/\alpha^2)] + \ell\,\beta^{2\ell}\gamma^2\beta^2/\alpha^2 \\
&- \ell\,(1 - \ell)\,\alpha^{2\ell}\gamma^2\beta^2/\alpha^2 = 0,
\end{aligned}$$

where $\alpha = A_1/A_2$ and $\beta = B/A_2$ in the general case. This equation is solved by means of the Cardan formula, and the imaginary part of σ (the growth rate of the perturbation) is extracted.

The results are shown on figure 2 (plate 1), for $\Gamma_t = 0$ ($\gamma = (\alpha^2 - 1)/\beta^2$). On figure 2($a$), we delimit the regions in the ($\alpha > \beta$) semi-plane where wavenumber ℓ (of between 2 and 8) is the most unstable. On figure 2(b), we plot the corresponding growth rate versus α and β. On figure 2(a) we observe that the larger the wavenumber, the narrower the region where it dominates. This region can be clearly identified for wavenumbers $\ell = 2$ to $\ell = 5$ and with more difficulty for $\ell = 6$ and beyond. For each of the $\ell = 2$ to $\ell = 5$ wavenumbers, the peak in growth rate is well marked and well separated from the maxima for any other ℓ. This is obvious for $\ell = 2$ and $\ell = 3$ on figure 2(b), but it can be shown for all wavenumbers up to $\ell = 5$ by superimposing charts of modal growth rates. Therefore, for a given value of (α, β) and for $\ell \leqslant 5$, only one mode of perturbation will distinctly grow on a given three-contour Rankine vortex and a specific multipole should be formed.

3.2. *Nonlinear evolution of a perturbed vortex in a contour surgery and a pseudospectral code*

We now present the formation of multipoles from perturbed three-contour Rankine vortices. We initialize the contour surgery code described in §2 with the mean flow stated in §3.1. On this circular vortex we create a modal deviation with 0.001 amplitude on each contour. We run three cases for each of which a single wavenumber ℓ dominates: (R1) $\alpha = 0.63, \beta = 0.35, \ell = 2$; (R2) $\alpha = 0.81, \beta = 0.4, \ell = 3$; (R3) $\alpha = 0.85, \beta = 0.4, \ell = 4$. For each case, the total circulation is initially null, so that $\gamma = (\alpha^2 - 1)/\beta^2$. The time step is 0.02 for numerical stability; the surgery threshold parameter $\mu = 0.15$ corresponds to a discretization into 160 nodes initially and roughly 1000 nodes at late stages (when the multipole is formed with peripheral filaments). The vorticity maps in the (x, y)-plane are presented on figure 3.

Owing to the small amplitude of the initial perturbation (one thousandth), we can accurately observe the linear stage of the instability (second frame of each line of figure 3). During this period, the disturbance grows on each contour with a phase shift characteristic of barotropic instability. A modal analysis (not shown here) reveals that the maximum modal amplitude is slightly larger for case (R1) than for case (R3): mode $\ell = 2$ has a more marked linear instability than $\ell = 4$, and even more so for higher wavenumbers than $\ell = 4$. Thus high-wavenumber perturbations develop less rapidly, their harmonics can amplify nonlinearly and the more complex multipoles are more rarely produced. Here, after 7 or 8 dimensionless time units, the nonlinear effects have taken place and the multipoles are clearly formed: the periphery has condensed into ℓ poles. From the original outer annulus, the most sheared parts now form filamentary debris, which later interact with the satellites and are slowly

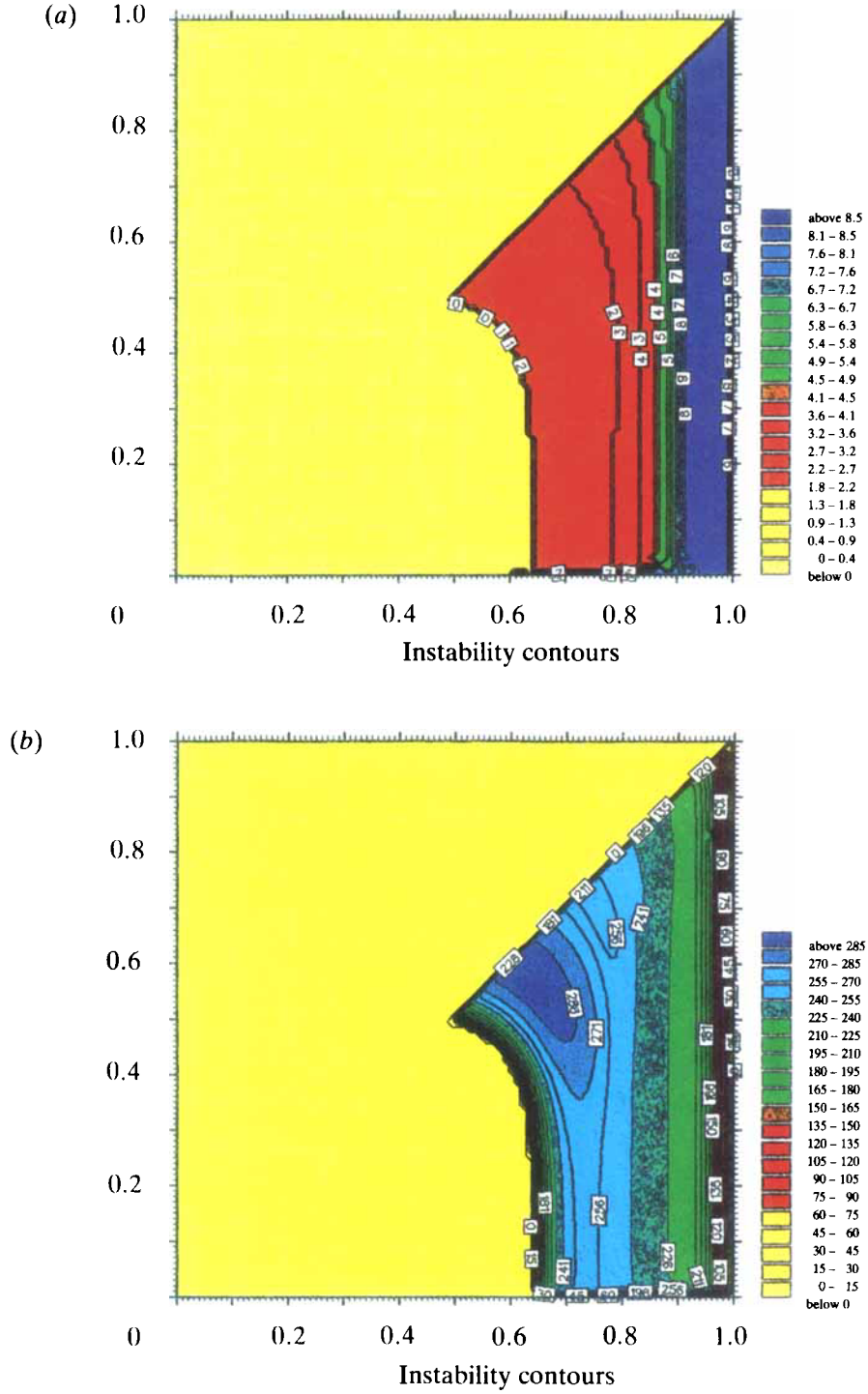

FIGURE 2. Linear stability diagrams of the three-contour Rankine vortex with $\Gamma_t = 0$ in the (α, β) semi-plane: (*a*) chart of most unstable wavenumber, for modes $m = 2$ to $m = 8$; (*b*) maximum growth rate (multiplied by 1000) for modes $m = 2$ to $m = 8$.

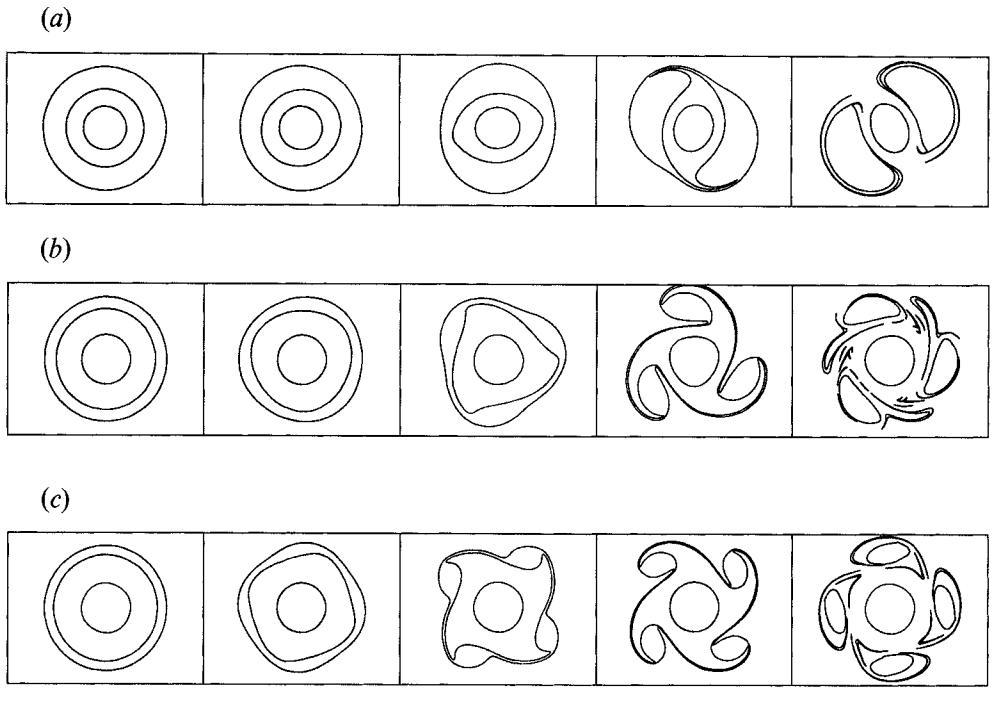

FIGURE 3. Nonlinear evolution of a slightly perturbed three-contour Rankine vortex in a contour surgery code: (*a*) circular vortex with $\alpha = 0.63, \beta = 0.35, \Gamma_t = 0, \ell = 3$ at times $t = 0, 5, 8, 9, 10\tau$; (*b*) same as (*a*) but for $\alpha = 0.81, \beta = 0.40, \Gamma_t = 0, \ell = 3$ at times $t = 0, 4, 5, 6, 8\tau$; (*c*) same as (*a*) but for $\alpha = 0.85, \beta = 0.40, \Gamma_t = 0, \ell = 4$ at times $t = 0, 6, 8, 9, 11\tau$.

dissipated as they shrink under the surgery scale. But this threshold is small and the dissipative timescale long compared to the eddy turnover period. We do not show the whole development of this 'viscous' adjustment process for this run because the numerical cost and CPU time of computations grow as N_{nodes}^2, with $N_{nodes} \sim 1000$ for $\mu = 0.15$.

To fully observe the nonlinear stage, we have run case (R2) with $\mu = 0.20$ and $\mu = 0.25$ (an increasing dissipation) and a larger initial perturbation amplitude (1%). These two simulations present no qualitative difference and only the first is shown on figure 4(*a*). Two periods appear in the nonlinear stage: first, during the adjustment ($t \leqslant 15\tau$, where τ is the core turnover period, $\tau = 4\pi/\gamma$), filaments formed by the initial annulus induce strong displacements and deformations on the satellites. Then, after $t \sim 15\tau$, most small-scale debris has been dissipated; the multipole thus formed is still robust at $t \sim 60\tau$. To complement this observation, we plot on figure 4(*b*) the amplitudes of the azimuthal modes of perturbation versus time, for the run of figure 4(*a*). The fundamental mode $\ell = 3$ grows exponentially, for a period of roughly 3τ, before the first harmonic (wavenumber 2ℓ) appears. This delay clearly suggests an origin of mode 2ℓ in wave–wave interaction and confirms the dominant growth of the fundamental mode (wavenumber ℓ). In both cases ($\mu = 0.20$ and $\mu = 0.25$), the adjustment process roughly takes 15τ, the final amplitude of mode $\ell = 3$ is 10%, but the damping effects are obviously larger in the second case ($\mu = 0.25$). We check that both the energy and angular momentum are reasonably well conserved (less than 1% variation), while the enstrophy undergoes a 9% decrease.

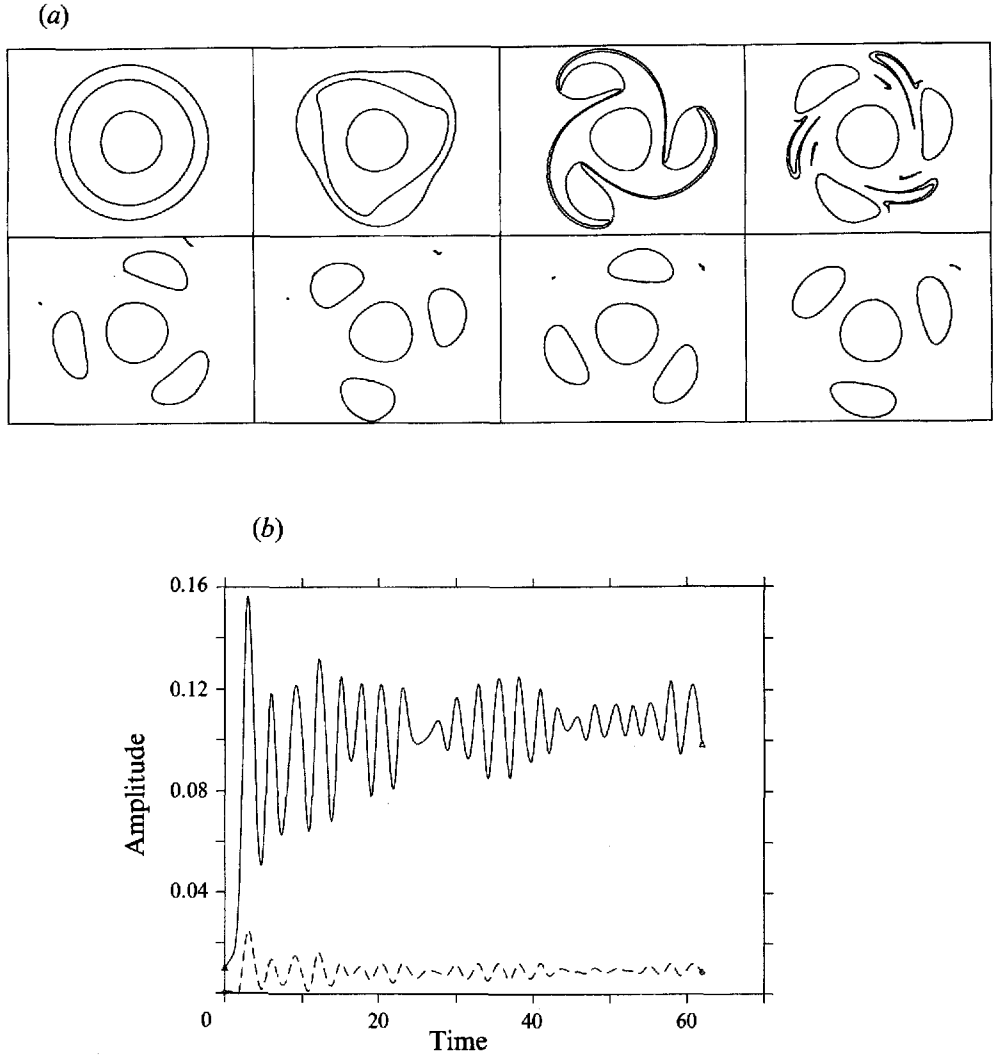

FIGURE 4. Rerun of simulation shown on figure 3(*b*) with a lesser surgery efficiency ($\mu = 0.20$ instead of $\mu = 0.15$). (*a*) Time evolution of the vorticity maps, times shown are $t = 0, 4, 6, 10, 38, 40, 42, 44\tau$. (*b*) Time series of azimuthal mode variations for the evolutions shown on (*a*); solid (dashed) line is the amplitude of mode $\ell = 3$ ($2\ell = 6$).

One could question the necessity of infinite gradients in the original vortex to form multipoles. To support the generality of this formation process, we now produce a pseudospectral simulation of case (R2). The initial vortex is similar to that used in contour surgery, scaled by a factor 2π in amplitude, and where the vorticity gradients have been replaced by an $\exp(-r^6)$ variation on a few gridpoints around $r = \beta$, $r = \alpha$ and $r = 1$. The horizontal resolution is 256 gridpoints in each direction. The initial amplitude of the $\ell = 3$ perturbation is again 0.1%. The vorticity plots are shown on figure 5. As the initial disturbance is weak, the linear stage is long (8τ), as in the contour surgery simulation. In the nonlinear evolution, filaments are produced as the remnants of the initial external annulus and wrap around the satellites, a

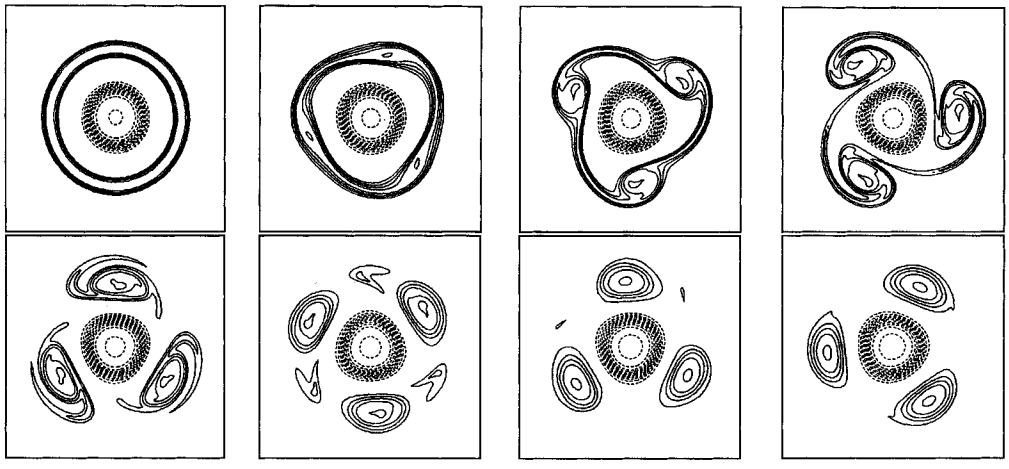

FIGURE 5. Nonlinear evolution of a slightly perturbed three-contour Rankine vortex ($\alpha = 0.81, \beta = 0.40, \Gamma_t = 0, \ell = 3$) in a pseudospectral code with $N_x = N_y = 256$, $\nu = 10^{-8}$; times shown are $t = 0, 3.6, 4.4, 5.2, 6, 7.2, 11.5, 15\tau$.

phenomenon already observed in tripole formation. The small orbiting fragments are progressively erased by the hyperviscosity and the whole structure finally stabilizes with three semicircular satellites. All these processes are identical to those observed in contour surgery, though with unequal timescales due to a different dissipation mechanism. This quadrupole is also strikingly similar to that formed by adding a strong mode $\ell = 3$ perturbation on a two-contour Rankine monopole (figure 4 of Carton 1992).

This pseudo-spectral simulation is first analysed in terms of integral quantities: circulation, angular momentum, energy, enstrophy; their time series are presented on figure 6. The circulation is well preserved; its total variation is shown on figure 6(*a*). The relative changes in angular momentum and energy are minor (respectively 2×10^{-4} and 2.7×10^{-3}). We consider that these three quantities are globally conserved. Enstrophy decreases by 10.7%. This proportion is similar to that found with the contour surgery simulation (R2). Though modest, it is still larger than the energy and angular momentum variations. Enstrophy decreases as the filaments ejected during the multipole formation are progressively erased by the hyperviscosity. Multipoles emanating from circular vortices thus appear as lower-enstrophy states with given integral constraints, confirming a previous hypothesis (Leith 1981). The physical consequences of the conservation of integral properties will be addressed in § 6.1.

As a final analysis, we verify that the multipole formed on figure 5 has reached a nearly invariant configuration. We recall that a stationary solution of the Euler equation is characterized by a biunivocal relation between the vorticity and the streamfunction in the rotating frame of reference. Therefore we determine experimentally the global rotation rate of the multipole, $\Omega = -0.058$ (note that the point-vortex equivalent is $\Omega_{pv} = -0.057$), and on figure 7 we plot the vorticity ζ versus the corotating streamfunction $\psi_c = \psi - \Omega r^2/2$ for the final quadrupole. The scatter plot is coherent despite a little dispersion close to the zero-vorticity level. Thus this quadrupole is a stationary equilibrium solution of the Euler equation. We also remark that such nonlinear (ζ, ψ_c) relations have been previously observed for a tripole (Orlandi & van

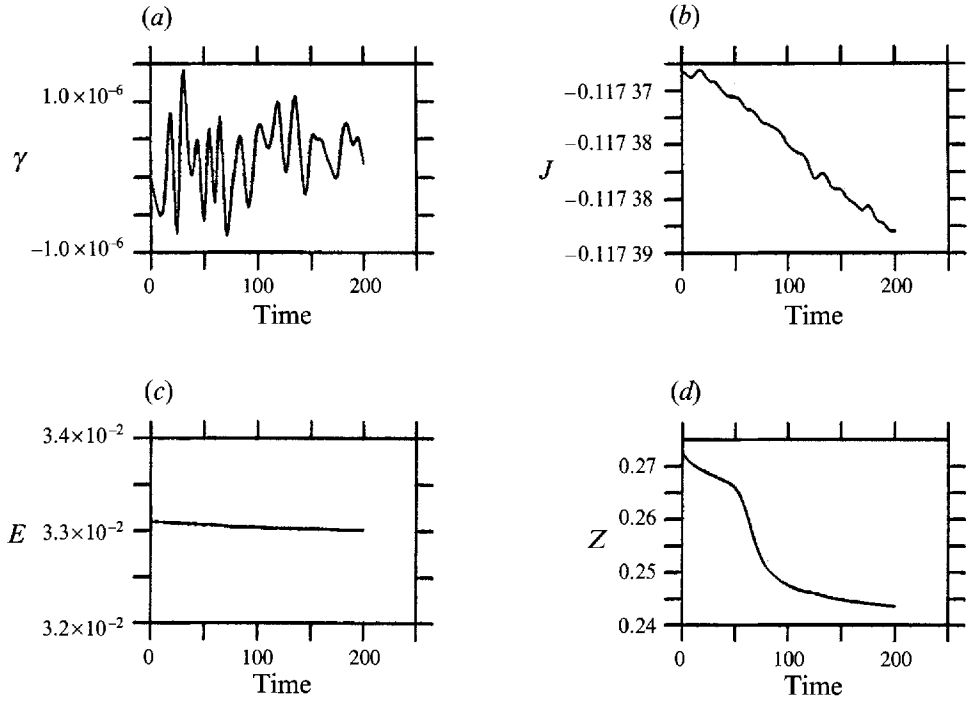

FIGURE 6. Time series of the integral quantities during the run shown on figure 5: (*a*) circulation, (*b*) angular momentum, (*c*) energy, (*d*) entrophy.

Heijst 1992) and for a quadrupole (Carton 1992). However, no conclusion on the stability of this multipole can yet be inferred from the mathematical form of this relation.

4. Multipolar equilibria

4.1. *Analytical developments*

In the previous section, we have shown how unstable monopolar vortices can transform into relatively long-lasting multipolar aggregates. In this section, we study multipoles as generic equilibria of the Euler equation ((2.1) with $\nu = 0$). At the end of this section we will compare these equilibria with the multipolar end-products of the unstable evolutions previously described. On figure 1(*c*), we give a schematic representation of a quadrupole. We call $r_c = (1 + a)/2$ the distance betweeen the core and the satellite centres and $r_a = (1 - a)/2$ the satellite radius. Any number N of satellites could be considered, but for 7 or more of them, point-multipoles are not stable when the core and the satellites have opposite-sign polarity (Morikawa & Swenson 1971).

Here we derive analytically the form of symmetric multipolar equilibria: we assume that the size of each vortex patch composing them is small compared to the distance separating the patches. To exhibit the shape of the steady states, we apply the technique described in Appendix A. The absolute velocity can be expressed by (2.2). In this equation we set $\gamma_k = \gamma$ for the core vortex and $\gamma_k = \gamma_0$ for the satellites. Then we write that the vortex boundaries are streamlines in the corotating frame

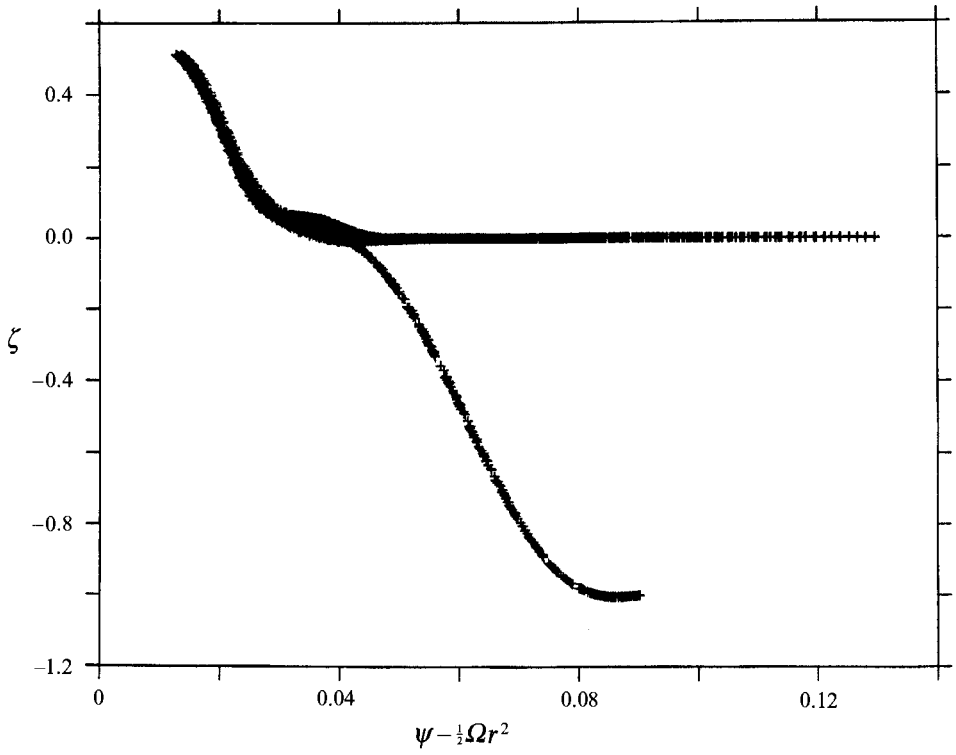

FIGURE 7. Vorticity versus corotating streamfunction for the quadrupolar state of the run of figure 5; $\Omega = -0.058$.

of reference and we perform an expansion of the angular velocity Ω and of the boundary $\rho_k(\theta)$ of the kth vortex patch in powers of the small geometrical parameters $\delta_a = (1-a)/(1+a)$ and $\delta_b = 2b/(1+a)$ (see Appendix A). We obtain

$$\Omega = \left(\gamma \frac{\delta_b^2}{2} + \gamma_0 \delta_a^2 \frac{N-1}{4}\right)(1+\delta_a^2\,\omega_0) = \Omega_0\,(1+\delta_a^2\,\omega_0) \tag{4.1}$$

with ω_0 the correction to the point-multipole angular velocity Ω_0 (see Appendix A). Now the core boundary is defined by

$$\rho_b = b\,[1 + k_0\,\delta_b^N\,(\cos(N\theta - 1)] \tag{4.2}$$

and the satellites are bounded by

$$\rho_a = r_a\,[1 + k_1\,\delta_a^2\,\sin^2(\theta) + k_2\,\delta_a^3\,\sin^2(\theta)\,\cos(\theta) + \delta_a^4\,(\mu + \nu\cos^2(\theta))\,\sin^2(\theta)]. \tag{4.3}$$

All constants k_0, k_1, k_2, μ, ν are given in Appendix A.

The rotation rate is not essentially altered by finite-area effects. The core boundary presents N maxima directed between the satellites; these latter resemble orthoradial ellipses at first order. Obviously we cannot infer any limitation on the existence of equilibria from these asymptotic formulae. Still they give satisfactory results even for finite δ_b and δ_a as we will see in the following subsection and they have the advantage of generality compared to a case-by-case numerical study.

4.2. *Numerical results*

Multipolar equilibria are numerically obtained by means of a relaxation algorithm designed by Wu, Overman & Zabusky (1984). This technique has already been used to exhibit tripolar steady states (Polvani & Carton 1990). It is based on (2.2); it relaxes the boundary to render the velocity tangential at each node and achieves second-order precision in the positions of the nodes on each vortex boundary and for the global rotation rate Ω. We initialize this routine with $N+1$ small circular vortices for the first step (with given a and b). The following iterations (when we increase b or decrease a) start from the previous equilibrium contours, scaled by the b_{new}/b_{old} (or $(1-a_{new}/1-a_{old})$ ratio. The total circulation is kept zero, so that the vorticity γ of the core is readjusted at each step ($\gamma_0 = 1$ for the satellites).

On figure 8 we show some numerical equilibria for $N = 3$, 4 and 5 and $\Gamma_t = 0$. Tripoles ($N = 2$) have been presented in a previous work and are not detailed here (Polvani & Carton 1990). Contrary to what is sometimes observed for $\Gamma_t \neq 0$, the core vortex is not extremely deformed; indeed, its vorticity balances the shear exerted by the satellites as the total circulation is null. More specifically the core boundary does not exhibit cusps between the satellites: it would require very small steps in a or b to attain limiting states with cusps. As for satellites, they are smaller in the more complex multipoles. This could be explained by the necessity to avoid merger of the like-signed satellites which are then more closely located. Unfortunately this simple argument does not take into account the shear exerted by the core vortex and proves inaccurate quantitatively. The physical explanation lies in the geometrical structure of a stationary state: for the vorticity distribution to be invariant, it must lie between the separatrices of the corotating streamfunction ψ_c (see figure 1*d*). These separatrices join at the saddle points X_h, Y_h of ψ_c, which are as many as the number N of satellites. Moreover, with more satellites, the core vortex circulation is more intense and brings the separatrices closer to one another. Therefore, the area between separatrices (thus bounded by $\psi_c = \psi_c(X_h, Y_h)$) is increasingly smaller with larger N (see figure 1*d* for the comparison of the area bounded by (X_{h1}, Y_{h1}) and (X_{h2}, Y_{h2}), which is larger in a quadrupole than in an hexapole). Consequently we will not investigate in detail hereafter multipoles with more than five satellites, nor structures with very small and distant cores and peripheral vortices. Such aggregates have little chance to form in a turbulent fluid where vortices mutually interact by a weak strain.

On table 1 we compare the analytical and numerical steady states. We compute the relative differences between the analytical and the numerical results for several geometrical and physical quantities: the core and satellite areas, the angular velocity of the multipole, the amplitudes of the mode-N deviation of the core boundary and of mode 2 on the satellite boundaries. The first row of figures is given as a reference; it corresponds to small core and satellites. In this case, all relative errors remain bounded by approximately 1%. All other diagnostics correspond to the steady states shown on figure 8. They remain satisfactory even for large cores, but for the amplitude of the central mode N. This is due to extremely large values of b (0.4–0.5) and can be explained as follows: for a large core area with a given circulation, the core vorticity is weak compared to the satellites; therefore the shear at the centre is larger and the mode-N deformation is more intense than that computed by a perturbation expansion. Still, most discrepancies are bounded by roughly 40%, a satisfactory figure in view of the constraining hypotheses. The analytical method is proved robust and more general than the numerical procedure. Using the previous results, we can now check that multipoles formed from unstable three-contour Rankine vortices

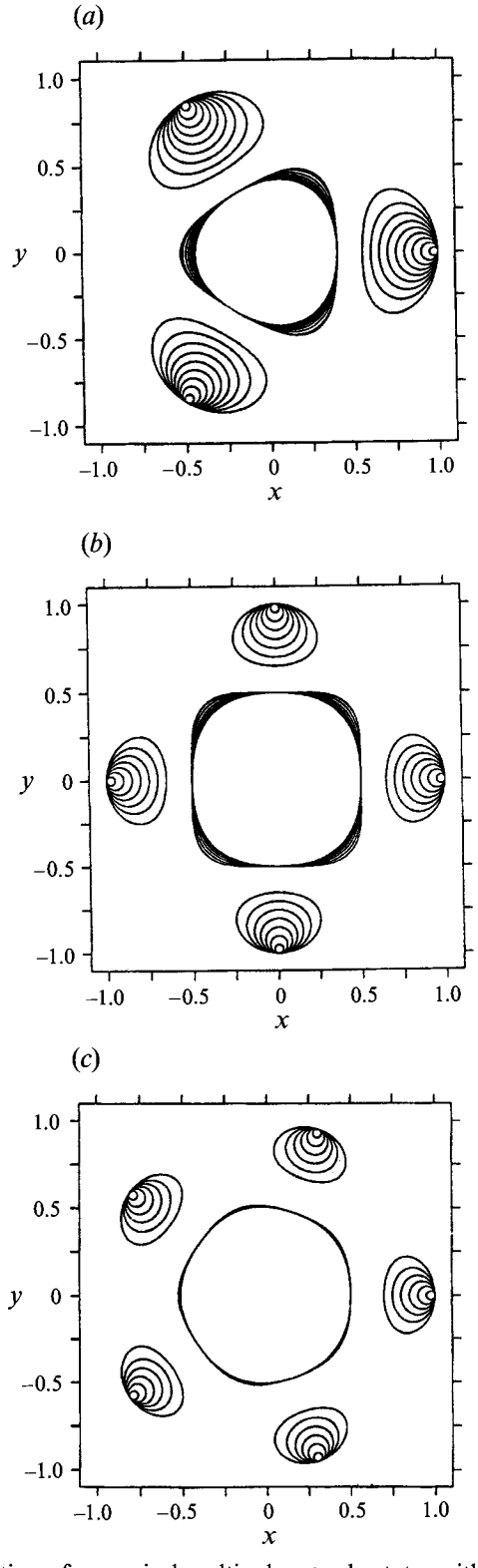

FIGURE 8. A selection of numerical multipolar steady states with $N = 2, 3, 4(a\text{–}c)$; $\Gamma_t = 0$.

a	b	N	$\frac{DA_1}{A_1}$	$\frac{DA_2}{A_2}$	$\frac{D\Omega}{\Omega}$	$\frac{Dm_c}{m_c}(N)$	$\frac{Dm_s}{m_s}(2)$
0.90	0.1	3	1×10^{-5}	2×10^{-4}	1.5×10^{-2}	1×10^{-2}	1.4×10^{-2}
0.95	0.4	3	2×10^{-2}	-5×10^{-5}	-2.5×10^{-3}	2.7×10^{-1}	-1.4×10^{-2}
0.75	0.4	3	6×10^{-2}	9×10^{-3}	9×10^{-2}	3.9×10^{-1}	7.5×10^{-2}
0.55	0.4	3	1.1×10^{-1}	2.0×10^{-1}	3.5×10^{-1}	5×10^{-1}	3.6×10^{-1}
0.95	0.5	4	2×10^{-2}	-4×10^{-5}	-4×10^{-4}	2.8×10^{-1}	-1×10^{-2}
0.80	0.5	4	3×10^{-2}	6×10^{-3}	8×10^{-2}	3.8×10^{-1}	6×10^{-2}
0.65	0.5	4	8×10^{-2}	1.1×10^{-1}	2.8×10^{-1}	4.9×10^{-1}	2.7×10^{-1}
0.95	0.5	5	4×10^{-3}	2×10^{-3}	6×10^{-3}	0.17	-2×10^{-3}
0.80	0.5	5	8×10^{-3}	1.6×10^{-3}	1.2×10^{-1}	2.2×10^{-1}	1.2×10^{-1}
0.70	0.5	5	7×10^{-2}	1.4×10^{-1}	3.2×10^{-1}	1.8×10^{-1}	3.5×10^{-1}

TABLE 1. Comparative diagnostics of numerical steady states of figure 8 with their analytical counterparts: areas, angular velocity, modal amplitudes of contour deformation.

are relatively invariant structures. We consider the quadrupole obtained after the adjustment in run (R2) (with $\mu = 0.20$) and average it in a reference frame rotating with the vortex. This quadrupole is relatively invariant but for a slight satellite wiggling and deformation. The horizontal scale of the quadrupole is 1.12 times that of the original vortex; it shows that the peripheral vorticity moves outwards while compacting into satellites. This is due to the conservation of angular momentum. After normalization of the outer radius to unity, we get $b = 0.343, a = 0.584$. On figure 9, we compare this multipolar end-product to the numerical equilibrium, with the same geometrical parameters. The similarity is reasonable but for a moderate shift in one of the satellite centres; the asymmetric modes have therefore not yet been completely damped by the weak surgery effect in run (R2). We can conclude that the instability of three-contour Rankine vortices produces multipoles similar to steady states.

5. The stability of multipolar steady states

We now have to determine which, if any, of these steady states are stable as well as the results of possible decay. We will first determine the linear stability of multipolar vortices. We will then run nonlinear simulations with the multipolar equilibria as initial conditions. Finally we will perturb these multipoles either initially or with a permanent strain field.

5.1. *Linear stability*

According to Morikawa & Swenson (1971), seven (or more) point vortices always form an unstable configuration around a core vortex of opposite polarity. Now if the total circulation is assumed null, then (with Morikawa & Swenson's notation) the satellite circulation $\Gamma_0 = 1$, the core circulation $\Gamma = -N$ and only tripoles and quadrupoles can meet the stability condition.

Here we compute the stability of a multipole composed of a central circular vortex and point satellites. Each satellite can undergo a radial or azimuthal motion of exponentially growing amplitude and the core vortex boundary is deformed by a wave with wavenumber p and a similar time-dependence. Then the dynamical equation (2.1) is linearized and the velocity formula (2.2) is computed with all contributions (core and satellite vortices). After some rather tedious algebra, three coupled equations are

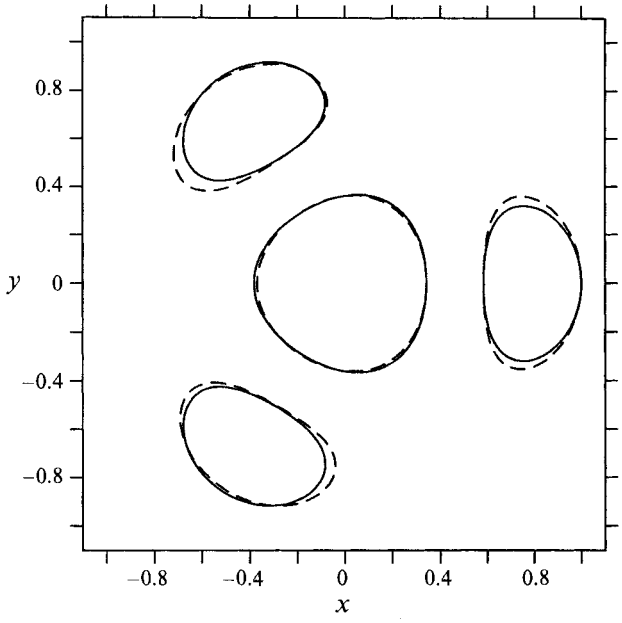

FIGURE 9. A comparison of the multipole produced by the instability of the circular vortices of figure 3 (- - - -) with the equilibria corresponding to the same parameters (——).

obtained, each one linear in σ_p, the growth rate of azimuthal mode-p perturbation. One equation corresponds to the radial displacement of the satellites, one to their azimuthal motion, the last one to the deformation of the core. Successive eliminations finally yield a third-order equation in σ_p for the instability of the whole multipole:

$$\sigma_p^3 - \omega_p\sigma_p^2 + (A_pB_p + 2K_p)\sigma_p - \omega_pA_pB_p - K_p\Omega = 0, \tag{5.1}$$

with Ω the rotation rate and

$$\begin{aligned}
\omega_p &= (\gamma - 2\Omega + \Gamma_0/\pi r_c^2)p/2 + \gamma/2,\\
A_p &= \Gamma_0(N - 1 + (N - p - 1)(p - 1))/(4\pi r_c^2),\\
B_p &= -\gamma\delta_b^2 + \Gamma_0(1 - N + (N - p - 1)(p - 1))/(4\pi r_c^2),\\
K_p &= \Gamma_0 N p\delta_b^{2p}/(8\pi r_c^2),
\end{aligned}$$

where $\gamma = \Gamma/\pi b^2$ is the core vorticity, b is the radius of the core , r_c is the distance of the satellites from the centre and $\delta_b = b/r_c$ (for more details, see a similar derivation by Acton & Dhanak 1993). It can be shown that the deformation of the core vortex corresponds to the steady state previously computed. Considering the initial vortex as circular is thus equivalent to neglecting $O(\delta_b^N)$ terms. This third-degree equation must have three real roots for stability. In fact, its solution is not qualitatively different for point-multipoles and for these desingularized vortices. When $K_p = 0$ the point-multipoles result is restored and the equation becomes

$$(\sigma_p - \omega_p)(\sigma_p^2 + A_pB_p) = 0.$$

In that case we get the stability criterion for point multipoles $A_pB_p \leqslant 0$, which leads

to $\Gamma/\Gamma_0 \geqslant -(N-1-(N-p-1)(p-1))/4$. It has also been checked that when $\Gamma = 0$ the original results by Thomson (1883) are found.

Some rapid algebra on these formulae shows that N-poles are mostly unstable on wavenumber $p = E(N/2)$, where $E(x)$ is the integer part of x. Multipoles with an even number of satellites should thus degenerate into twice as simple multipoles, while 'odd-N' multipoles should undergo an asymmetric decay. Still, this simple formula does not take finite-area effects into account, which play an essential role in merger or dipolar breaking. A complete analysis of the linear stability of the multipolar equilibria has been undertaken, but as of now, its results do not fit the nonlinear numerical simulations and will not be shown here.

5.2. *Nonlinear evolution of multipolar equilibria*

We now consider the nonlinear evolution of the previous multipolar steady states. As a first test of stability, we initialize the contour surgery code with the multipolar equilibria previously obtained. These multipoles are unperturbed and evolve in free-decay. We set $\mu = 0.12$ to avoid excessive dissipative effects, except when specified. On table 2, we present the results of the nonlinear simulations for 30 multipoles with zero total circulation; approximately 60 more cases with finite circulation have been studied which did not show qualitative differences and are not detailed here (Morel & Carton 1991). We also refer the reader to the previous study on tripoles (Polvani & Carton 1990) for supplementary material.

Table 2 clearly shows that most tripolar and quadrupolar equilibria are stable ($N = 2, 3$). Such a stable quadrupole evolution is presented on figure 10(a), where $a = 0.55, b = 0.40, \Gamma_t = 0$. It confirms Morikawa & Swenson's stability prediction for point-tripoles and point-quadrupoles. It is also consistent with the dominant instability of wavenumber $p = E(N/2)$. Indeed, mode $p = 1$ perturbations are relatively stable on barotropic vortices; they are manifested by a translation of the multipole or by its destruction as the core vortex pairs with one of the satellites, though usually only under a rather intense forcing. The asymmetric mode $p = 1$ is far less unstable than the elliptical mode $p = 2$ which appears on multipoles with $N \geqslant 4$.

Elliptical deformations either lead to the formation of a tripole or to dipolar breaking. The $p = 2$ mode will appear predominantly on multipoles with $N = 4$ or $N = 5$. If $N = 4$, the result will be a symmetric tripole or two dipoles. If $N = 5$, the final state will be strongly asymmetric. Tripoles form by (successive) satellite mergers when the core is sufficiently small and strong to resist the shear exerted by the satellites. Conversely, on a core with a larger area, hence with a smaller vorticity, this shear induces a large elliptical deformation resulting in dipolar breaking. A similar result, though still with relative numerical accuracy, is obtained with the conservation of integral quantities (see § 6.2).

On figure 10(b), we present the tripole formation from an unstable pentapole with a small core ($a = 0.7, b = 0.3, \Gamma_t = 0$), and on figure 10($c$) the dipolar breaking of a more extended pentapole ($a = 0.65, b = 0.5, \Gamma_t = 0$). When satellites merge, filamentation is observed as usual in symmetric vortex merger. The expulsion of filaments from the core is observed more rarely, when wavenumbers $p = 2$ and $p = 3$ are simultaneously present. This occurs during the decay of the hexapole $a = 0.7, b = 0.4, \Gamma_t = 0$.

Finally, no axisymmetrization process occurred for the zero-circulation multipoles, such as that observed for the $a = 0.3, b = 0.2, \gamma = -4$ tripole (Polvani & Carton 1990). This is explained by the absence of multipolar steady states with satellites sufficiently large and close to merge: as the total circulation is null, the strain induced by the

Nsv	b	a	Nonlinear evolution
2	0.15	0.60	stable tripole
2	0.20	0.80	stable tripole
2	0.20	0.45	asym. breaking; 1 monopole & 1 dipole
2	0.25	0.60	stable tripole
3	0.20	0.55	stable quadrupole
3	0.20	0.80	stable quadrupole
3	0.25	0.75	stable quadrupole
3	0.30	0.55	stable quadrupole
3	0.35	0.55	stable quadrupole
3	0.40	0.80	slightly unstable quadrupole
3	0.40	0.55	stable quadrupole
3	0.45	0.80	stable quadrupole
4	0.15	0.80	stable pentapole(?)
4	0.20	0.65	satellite merger; tripole
4	0.20	0.70	satellite merger; tripole
4	0.25	0.70	satellite merger; tripole
4	0.30	0.70	satellite merger; tripole
4	0.40	0.70	core breaking; 2 dipoles
4	0.45	0.75	core breaking; 2 dipoles
4	0.50	0.65	core breaking; 2 dipoles
4	0.50	0.80	core breaking; 2 dipoles
5	0.20	0.70	satellite merger; asym. tripole
5	0.30	0.70	satellite merger; asym. tripole
5	0.40	0.70	satellite merger; asym. tripole
5	0.50	0.70	satellite merger; asym. quadrupole
5	0.55	0.80	asym. breaking
5	0.60	0.80	core breaking; dipoles

TABLE 2. Nonlinear evolution of a selection of 30 multipoles as observed in the contour surgery code.

core on the periphery is bounded. On the other hand axisymmetrization has been observed for multipoles with strong cores and $\Gamma_t \neq 0$.

To test further the stability of quadrupoles, we perform several simulations where the multipole is either initially or permanently disturbed. First, we subject the vortex to a stationary large-scale deformation field of the form

$$U = \eta x - \Omega y, V = \Omega x - \eta y,$$

where Ω is the background rotation and η the background strain field. A pure shear corresponds to $A = \Omega = -\eta$. To test the quadrupole stability, we select two geometrical cases, one with large core and satellites ($a = 0.55, b = 0.40, \Gamma_t = 0$), the other with smaller and more distant satellites ($a = 0.80, b = 0.45, \Gamma_t = 0$). The first case was extensively analysed and the results are presented in table 3. The second case showed a similar resistance, though on fewer tests.

On figure 11, we present the resistance of the quadrupole $a = 0.55, b = 0.40, \Gamma_t = 0$ to a permanent shear $A = \Omega = -\eta$. Table 3 states that $A = 0.09$ corresponds to the stability limit below which the vortex remains quasi-invariant and beyond which the quadrupole breaks asymmetrically. On figure 11(a), $A = 0.05$ and a mode $p = 1$ wave travels around the core boundary, eventually resulting in a cusp and a filament formation; on figure 11(b), $A = 0.10$ generates a larger displacement of the core

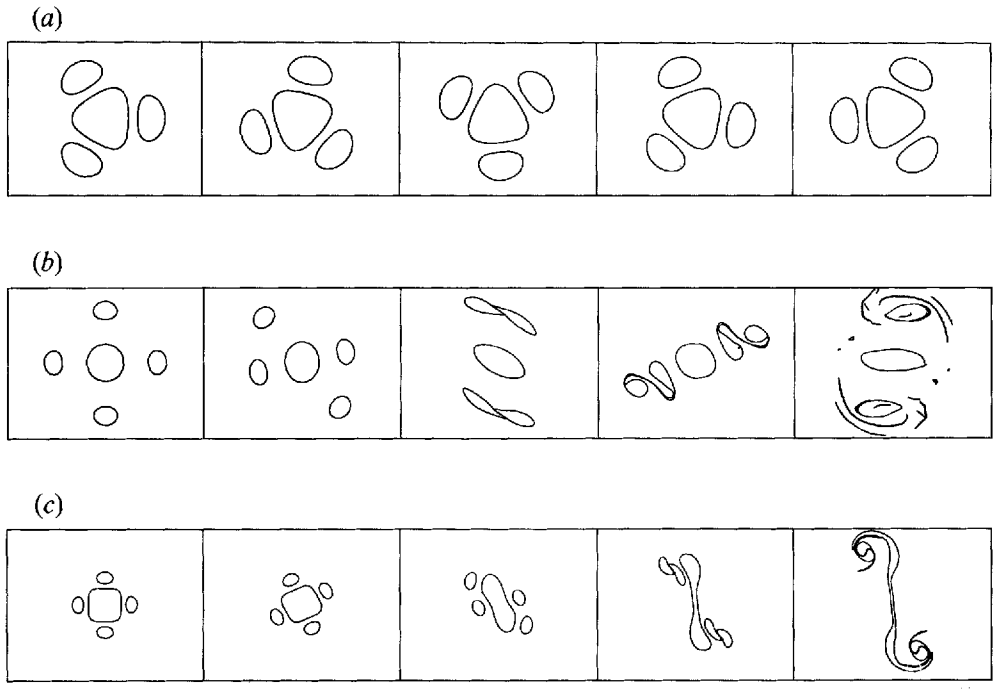

FIGURE 10. (*a*) Contour surgery evolution of a stable quadrupole $a = 0.55, b = 0.40, \Gamma_t = 0$ (unperturbed). Times shown are $t = 0, 6, 12, 18, 24\tau$. (*b*) Contour surgery evolution of an unstable pentapole $a = 0.7, b = 0.3, \Gamma_t = 0$ (unperturbed), satellite merger leading to tripole formation. Times shown are $t = 0, 33, 36, 39, 45\tau$. (*c*) Contour surgery evolution of an unstable pentapole $a = 0.65, b = 0.5, \Gamma_t = 0$ (unperturbed), core breaking forming dipoles. Times shown are $t = 0, 15, 18, 20, 22\tau$ (box scale twofold).

towards one satellite inducing a strong deformation of the latter. This configuration rapidly becomes irreversibly asymmetric as two satellites are advected closer to each other until they merge. Simultaneously, the core vortex becomes elliptical and forms a transient tripole with the two remaining satellites. Finally, the asymmetric instability of the tripole prevails and the system ends as a monopole and a dipole.

For pure strain forcing, the stability limit is slightly higher, between $\eta = 0.12$ and $\eta = 0.135$. Beyond this limit, a mode-2 instability is generated by the large-scale strain field and the end-products of the instability are dipoles formed by core breaking. These results are reminiscent of the stability of the Kida ellipse. We may wonder if large-scale fields with a different symmetry would act similarly on multipoles. Indeed, in the far-field interaction of two vortices, all azimuthal components of deformation are present. We thus consider the case of a strain field with 3-fold symmetry acting on the quadrupole of table 3:

$$U = 3\eta(y^2 - x^2), \quad V = 6\eta x y.$$

The stability of the quadrupole in this field is much weaker than for elliptical deformations as it breaks for strain amplitudes smaller than 1% of the vorticity. In the distant interaction of a vortex with a multipole, this latter may thus be destroyed by the weaker mode-3 component of the induced strain before it is affected by the elliptical deformation.

Finally we test the robustness of quadrupole $a = 0.55, b = 0.40, \Gamma_t = 0$ when

	Shear field, $\Lambda = \Omega = -\eta$
$\Lambda = 0.05$,	invariant quadrupole
$\Lambda = 0.05$ to 0.08,	stable quadrupole
$\Lambda = 0.09$,	stability limit
$\Lambda = 0.10$,	breaking into a dipole and a monopole
	Strain field, η
$\eta = 0.05$	quadrupole invariance
$\eta = 0.07, 0.08$,	slight filamentation
$\eta = 0.09$ to 0.12,	strong oscillations of core centroid
$\eta = 0.135$ to 0.15,	core breaking forming 2 dipoles
	Initial displacement dx of core centroid ($\epsilon = \mathrm{d}x/(a-b)$)
$\mathrm{d}x = 0.025; \epsilon = 0.167$	stable quadrupole, northward displacement
$\mathrm{d}x = 0.03; \epsilon = 0.20$,	strong deformation and northward displacement
$\mathrm{d}x = 0.04; \epsilon = 0.267$,	breaking into a monopole and a dipole
$\mathrm{d}x = 0.05; \epsilon = 0.333$,	breaking into 2 asym. dipoles
	White noise displacement of contour nodes
$\xi = 0.01$,	stable quadrupole ($\mu = 0.12$)
$\xi = 0.025$,	stable quadrupole ($\mu = 0.15$)
$\xi = 0.05$,	stable quadrupole ($\mu = 0.25$)

TABLE 3. Long-term nonlinear behaviour of a stable quadrupole ($N = 3, b = 0.4, a = 0.55$) under shear, strain, asymmetric perturbation or white noise alteration, as observed in the contour surgery code.

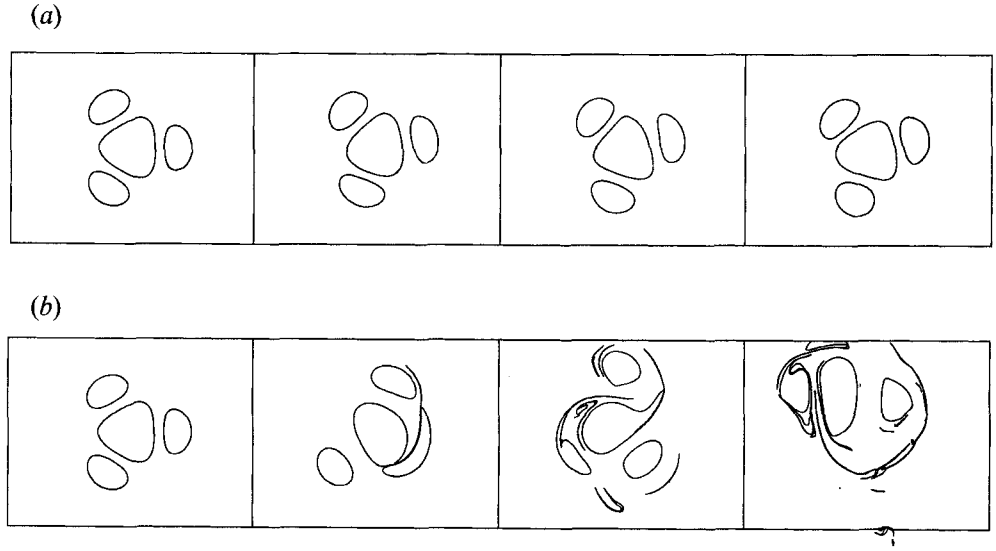

FIGURE 11. Evolution of quadrupole $a = 0.55, b = 0.40, \Gamma_t = 0$ under moderate shear; (*a*) $\Lambda = -0.05$ global invariance; times shown are $t = 0, 8, 16, 24\tau$. (*b*) $\Lambda = -0.1$ satellite merger and core pairing; times shown are $t = 0, 4, 8, 12\tau$.

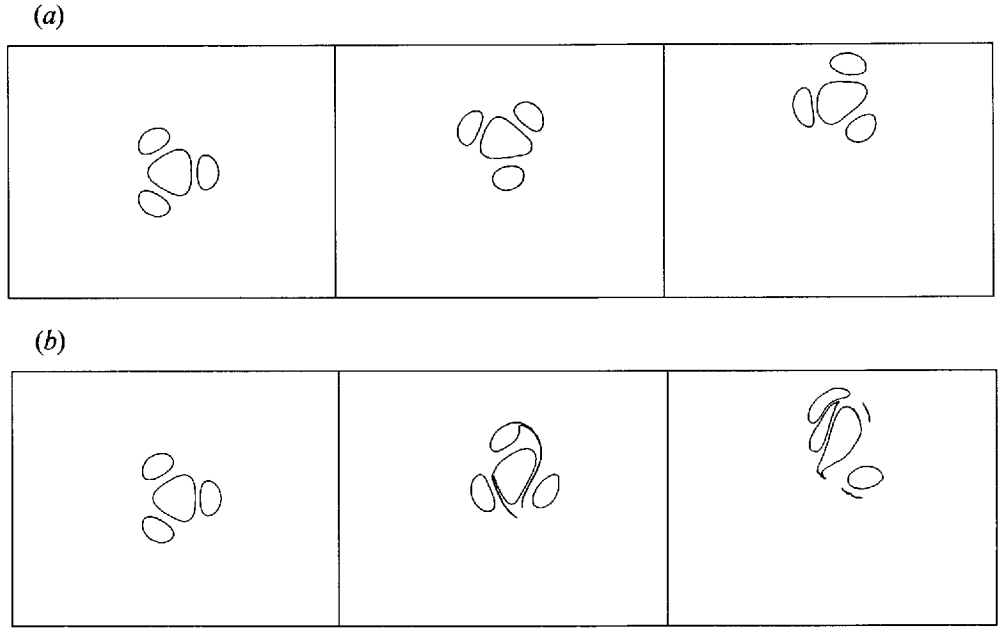

FIGURE 12. Asymmetric instability of quadrupole $a = 0.55, b = 0.40, \Gamma_i = 0$ induced by a core centroid displacement dx; (*a*) $dx = 0.025$ northward propagation; times shown are $t = 0, 12, 24\tau$ (box length is scaled by 1.5). (*b*) $dx = 0.05$ satellite merger and core pairing; times shown are $t = 0, 6, 12\tau$ (box length is scaled by 1.5).

initially perturbed. First, we add a mode-1 deformation by shifting the core centroid by a distance dx towards one satellite. The relevant dimensionless parameter is $\epsilon = dx/(a-b)$. For $\epsilon \leqslant 0.2$, the mode $p = 1$ deformation propagates on the core boundary and in the satellite locations, resulting in a northward displacement of the whole structure. Figure 12(*a*) shows this process when $\epsilon = 0.167$. Beyond $\epsilon = 0.25$, the whole structure becomes unstable: satellite merger and pairing with the core result in one dipole for $\epsilon = 0.267$ (figure 12*b*) while core breaking forms two dipoles for $\epsilon = 0.33$.

As a second type of initial disturbance, we displace all contour nodes by an amount $dx = \xi * rand(x), dy = \xi * rand(y)$, where *rand*() is a random number generator bounded by 0 and 1. This white noise contains all azimuthal wavenumbers and the most unstable should naturally emerge. This series of tests, though run in double precision, is less conclusive as the surgery scale μ must be augmented with ξ to avoid the formation of too many cusps. This increased 'viscosity' results in a smoothing of the initial disturbance, which renders the physical relevance of this numerical experiment questionable.

6. Integral constraints

From the previous observations in the numerical experiments, we now know that transformations from monopoles to multipoles or between multipoles produce final states with a slightly lower enstrophy, but similar energy, circulation and angular momentum, compared to the initial conditions. In order to compute analytically these integral constraints, we use the FAVR approximation for monopoles and

multipoles and assume that each vortex area and that the total angular momentum are conserved. As exact energy conservation is not simple to derive analytically, we will not use it extensively here. For each transformation, we first assume that enstrophy is conserved (by area conservation) and then show how a slight enstrophy decrease modifies the integral balances and their physical implications. All detailed calculations of the conservation laws are given in Appendix B for a three-contour Rankine vortex and for a generic multipole. In § 6.1, we present their physical consequences for the formation of a multipole from a three-contour Rankine vortex. In § 6.2, the transformation of a multipole into an other multipole is addressed.

6.1. *Multipole formation from a three-contour Rankine vortex*

We recall that, in the transformation of a three-contour Rankine vortex into a multipole, there is an outward motion of the satellite vorticity. With the conservation of area and angular momentum, computing the initial conditions from the final state is a straightforward problem. Conversely, we look here for the multipole characteristics r_a, r_c and b knowing the initial monopole (with radii A_1, A_2, B) and its most unstable associated mode N (see figure 1*c*). The result is obtained by inverting the conservation equations and by using a perturbation expansion in terms of the following small geometrical parameters:

$$\delta_A = \frac{r_A}{r_C} \text{ and } \delta_B = \frac{B}{r_C} \quad \text{with } r_A^2 = \frac{A_2^2 - A_1^2}{N},\ r_C^2 = \frac{A_2^2 + A_1^2}{2}.$$

All these quantities appear when we consider the equations at first order. We can then write

$$\begin{aligned} r_a &= r_A(1 - \tfrac{1}{2}k_{1o}\delta_A^2 + \alpha_1\delta_A^4), \\ r_c &= r_C(1 + \alpha_2\delta_A^2 + \alpha_3\delta_A^4), \\ b &= B(1 + k_o\delta_B^N), \end{aligned}$$

with k_{1o} and α_j defined in Appendix B.

The remarkable point is that the latter equations also give us an upper bound on A_1, A_2, B if a N-pole is to be found. Indeed, consider the first order for simplification and $A_2 = 1$; we must have $r_c \geqslant r_a + b$ (note that $r_a + r_c \neq 1$) to form a N-pole from the original monopole. Using the first-order perturbation expansion we get

$$B \leqslant \left[\frac{1 + A_1^2}{2}\right]^{\frac{1}{2}} - \left[\frac{1 - A_1^2}{N}\right]^{\frac{1}{2}} \text{ with } B \leqslant A_1.$$

We see that for a certain range of these parameters ($A_1 \approx B$), this equation cannot be satisfied. In that range of parameters, this is a sufficient condition to prevent N-pole formation. Outside that parameter range, complex multipoles ($N \geqslant 2$) can form, though dipolar breaking can still occur if the $p = 2$ mode is sufficiently unstable.

We now examine the effect of a slight enstrophy decay. When a three-contour Rankine vortex breaks into a multipole, the centre is not affected, only the outer annulus filaments and loses area. Thus the area conservation for the annulus becomes

$$A_{sat} = \pi(A_2^2 - A_1^2)(1 - \epsilon),$$

where ϵ is a small positive parameter representing the loss of area. This new equation

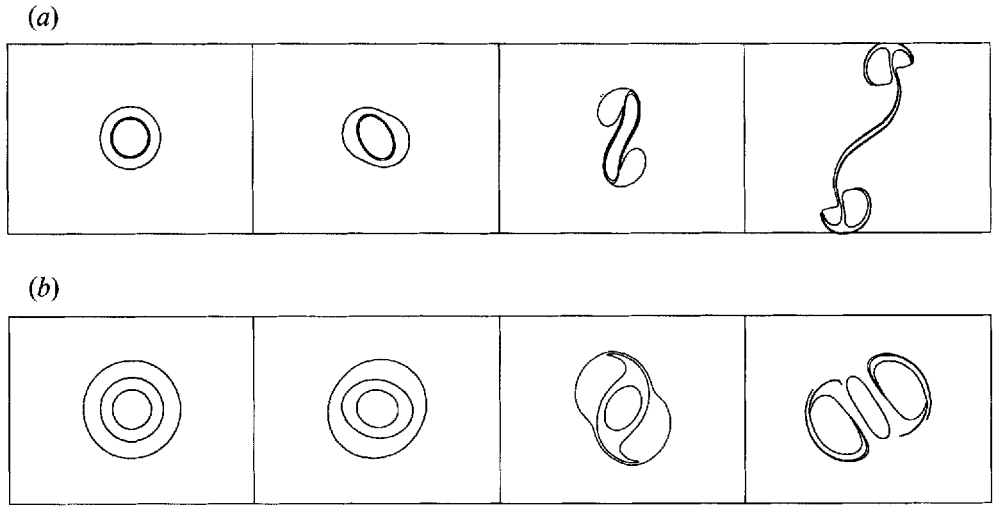

FIGURE 13. Contour surgery evolution of a zero-circulation three-contour Rankine vortex with a $\ell = 2, \epsilon = 0.001$ disturbance and $\mu = 0.15$: (*a*) $a = 0.65, b = 0.6$ producing dipolar breaking, times shown are $t = 0, 3, 4, 5\tau$ (box length scaled by 2.0); (*b*) $a = 0.65, b = 0.4$ with a tripole formation, times shown are $t = 0, 3, 4, 6\tau$ (box length scaled by 1.25).

yields at first order the following upper bound on B if a multipole is to be formed:

$$B_{lim} = \left[\frac{1+A_1^2}{2}\right]^{\frac{1}{2}}\left(1+\frac{\epsilon}{2}\right) - \left[\frac{1-A_1^2}{N}\right]^{\frac{1}{2}}\left(1-\frac{\epsilon}{2}\right).$$

Thus the effect of an enstrophy decrease (here via filamentation) is to favour multipole creation ($B_{lim} > B'_{lim}$ with enstrophy conservation). For instance, for $A = 0.65, N = 2, \epsilon = 0.1$ we obtain $B_{lim} = 0.37$. Numerical experiments show that with $B = 0.6$ the vortex slowly breaks into two dipoles (see figure 13*a*), while with $B = 0.4$ the core resists and a tripole is finally formed (see figure 13*b*). Our formula is thus slightly overevaluated, but it shows that the core and periphery of the original monopole have to be relatively distant to create multipoles.

6.2. *Multipole degeneracy*

As previously, we use the conservation of core and satellite areas and total momentum to forecast the result of a multipole instability. Contrary to §6.1, a zeroth-order approximation suffices here (the first-order correction makes only a few percent difference). The conservation laws are written

$$b_2 = b_1, \; N_1 r_{a1}^2 = N_2 r_{a2}^2, \; N_1 r_{a1}^2 r_{c1}^2 = N_2 r_{a2}^2 r_{c2}^2$$

if subscript 1 denotes the initial multipole and 2 the final state with fewer satellites. Thus the condition $r_{c2} \geqslant r_{a2} + b_2$ gives the following constraint on the initial multipole:

$$b_1 \leqslant \tfrac{1}{2}[1 + a_1 - (N_1/N_2)^{\frac{1}{2}}(1 - a_1)].$$

If this condition is satisfied, we can obtain a new multipole; otherwise the core breaks and forms dipoles. Again the condition is sufficient for dipole formation, but not for multipole creation. An example given on table 2 for $N_1 = 4, N_2 = 2, a_1 = 0.70$ gives $b_{lim} = 0.60$. We observe dipolar breaking for $b_1 = 0.40$. This might be due to a further

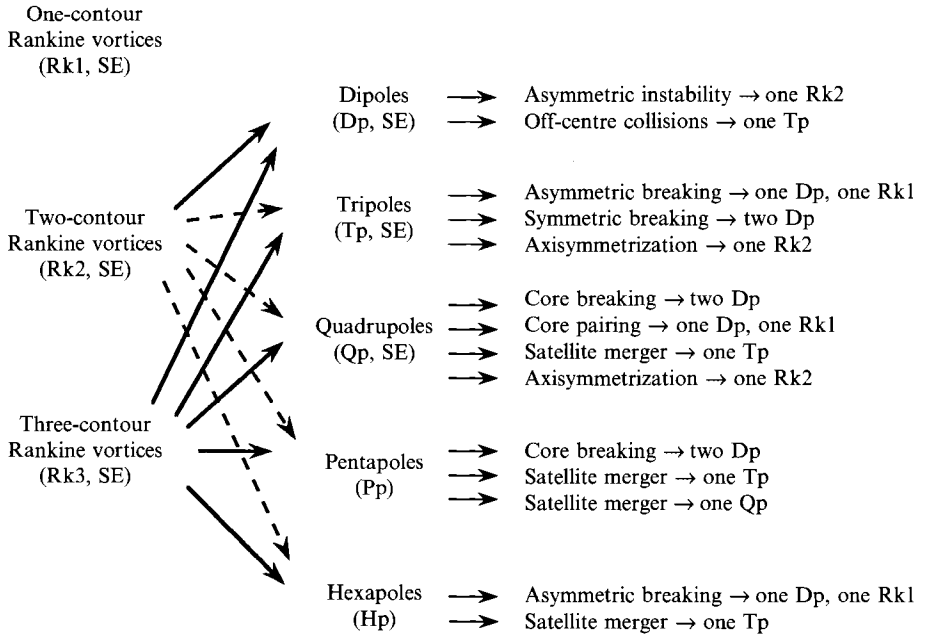

FIGURE 14. Synthetic diagram of the various vortex forms and of their respective transformations: solid thick arrows show a transition between vortex species with slight initial perturbation, while for dashed arrows, a strong initial disturbance is necessary for the transition to occur.

instability of a transient tripole on mode $p = 2$, or to a strong loss of enstrophy in filaments. We hope that a more complete analysis taking the energy conservation into account will help solve this discrepancy.

7. Summary and final conclusions

In this paper, we have addressed the question of the formation, existence and decay of isolated, piecewise-constant multipolar vortices. Circular step-like vortices with zero circulation easily transform into multipoles with fewer than six satellites by barotropic instability. This transition is favoured when the initial vorticity profile contains two separate active regions. The multipoles thus formed closely resemble the multipolar equilibria obtained by perturbation expansions around a circular shape, or via numerical relaxation procedures. On figure 14, we present the results of all nonlinear simulations performed with Rankine vortices and zero- or finite-circulation multipoles. The existence of stable equilibria for a vortex type is indicated by the symbol (SE). The stability analysis reveals that tripoles and quadrupoles are stable features of the multipolar vortex family, both naturally and when initially or permanently deformed. More complex multipoles decay into dipoles, tripoles (and seldom quadrupoles) by growth of elliptical (or triangular) deformations. Axisymmetric vortices can be end-products of these transformations, either after asymmetric breaking or after axisymmetrization (observed only for finite-circulation multipoles). The most frequent decay mechanisms are successive satellite merger, core breaking with dipole formation and core pairing with one satellite.

These evolutions are explained by the dominant instability of mode $p = E(N/2)$ for $N + 1$ point vortices. Thus the end-products of the evolutions will depend on the

initial parity of N (see table 4). If mode $p = 1$ is unstable, asymmetric instability will be manifested by a translation of the multipole or by core pairing with one satellite, while if mode $p = 2$ dominates, elliptical deformations will grow on multipoles. In fact, finite-area effects play a role as mode $p = 2$ finally leads to tripoles via merger or to dipoles via breaking. These finite-area effects can result in a dominance of dipoles or tripoles as final states instead of more complex multipoles. Finally, it appears that the conservation of integral quantities can help predict the final fate of an unstable vortex, though still more easily for a three-contour Rankine than for a multipole.

During the completion of this manuscript, a similar study by Carnevale & Kloosterziel (1994) was brought to our attention. This paper focuses on the instability of continuous shielded vortices, with two adjacent active regions and very steep vorticity gradients. It is of great interest to note that, starting from different conditions, our two studies converge to the same conclusion, viz. that quadrupoles are robust vortex structures. In their study, the numerical results are confirmed by laboratory experiments. At the same time, a study of tornadoes by Lin (1992) was mentioned to us by the two same authors. This contribution also shows the formation of multipolar vortices from initially circular vortices. It appears therefore that a multi-contour formulation is an appropriate method to describe the physics while keeping the number of parameters under control. Moreover, we have shown here that various techniques, such as analytical developments or numerical iterative schemes, contour surgery or pseudospectral codes, yield similar solutions with satisfactory accuracy.

Much work remains for multipole dynamics: relating the nonlinear (ζ, ψ_c) relation to stability and to minimum-enstrophy properties (as yet no analytical solution using perturbation expansions has been successful), obtaining a better numerical precision for the stability of multipolar steady states, using energy invariance to predict the decay of a multipole and relating dipole formation to successive instabilities of multipoles. We have provided here only a first glimpse of the problem. It is also of great importance to show the relevance of such work to geophysical flows. In particular, the effects of stratification on multipole dynamics are striking: the final states are oscillatory rather than steady and are dominated by cyclic potential energy exchanges (e.g. Carton & McWilliams 1989). A recent observation of baroclinic tripoles in the Bay of Biscay (by satellite I.R. imagery and *in-situ* data) confirms the model results (figure 2 of Pingree & Le Cann 1992). Using these oceanic parameters in a primitive equation model, they later showed that dipolar, tripolar and quadrupolar deformations alternate in the vortex shape. Transient tripolar forms have also been observed on a vortex drifting under the β-effect (Hesthaven *et al.* 1992). Finally, the presence of an isolated seamount has been shown to stabilize some multipoles in two-dimensional flows (Mied, Kirwan & Lindemann 1992; Carton & Legras 1994). When sufficient data on oceanic vortices are made available (e.g. by satellite observation), it would be of great interest to look for evidence of multipolar equilibria, especially in the vicinity of irregular coastlines.

The authors are very grateful to Dr D. G. Dritschel for his essential help, both in physics and numerics. Discussions with Drs G. R. Flierl, L. M. Polvani, B. Legras and J. C. McWilliams proved timely and valuable. Also, suggestions by two of the reviewers were quite helpful. Financial support for this work was provided by the Service Hydrographique et Océanographique de la Marine (France), under the research program 'Processus Associés aux Modèles Intermédiaires et Régionaux'. Computations were performed on IBM RS6000-550 and SGI R4000 workstations at SHOM/GRGS.

Appendix A. Multipolar equilibria

To derive the equation determining the stationary state in a rotating frame, we require that its contours must also be streaklines, viz. if $f(r,\theta,t) = f_j$ is the equation of the jth contour in the rotating frame, f must keep the same value all along the evolution:

$$\left.\frac{\mathrm{d}f}{\mathrm{d}t}\right|_{f(r,\theta,t)=f_j} = 0$$

or

$$\frac{\partial f}{\partial t} + \tilde{u}_r \frac{\partial f}{\partial r} + \frac{\tilde{u}_\theta}{r}\frac{\partial f}{\partial \theta} = 0,$$

where $\vec{\tilde{u}} = \vec{u} - \vec{\Omega} \times \vec{r}$ is the velocity in the rotating frame; $\vec{u}$ and $\vec{\Omega}$ are calculated using (2.2).

For a stationary state we have $f(r,\theta,t) = f(r,\theta) = r - g(\theta) = 0$ which leads to

$$\frac{1}{g(\theta)}\frac{\mathrm{d}g}{\mathrm{d}\theta} = \frac{\tilde{u}_r}{\tilde{u}_\theta}. \tag{A 1}$$

As $\vec{u}$ and Ω are calculated with (2.2), they also depend on the contours. This equation is too complicated to be solved in general and we can only get some approximation for g (= ρ_k hereafter, where k is the vortex index inside the multipole) and Ω using a small-parameter expansion. These parameters are the ratios of the vortex radii to their distance, δ_b and δ_a. We write

$$\Omega = \Omega_0 + \delta_k\,\Omega_1 + \delta_k^2\,\Omega_2..., \tag{A 2}$$

$$\rho_k(\theta) = \rho_{k0} + \delta_k\,\rho_{k1}\,f_1(\theta) + \delta_k^2\,\rho_{k2}\,f_2(\theta)... \tag{A 3}$$

with θ the local angle in the kth vortex frame of reference. To obtain the explicit values of the coefficients and of the form of the functions in the expansion (A 2) and (A 3), we use a generic technique that we detail hereafter for the core vortex.

Let us assume that

$$\rho_0 = b + \varepsilon h(\theta), \tag{A 4}$$

with $h(0) = 0$ because $\rho_0(0) = b$, where h and ε are to be determined. Equation (A 1) yields

$$\varepsilon h'(\theta) = \frac{u_r}{u_\theta - \Omega\rho_0(\theta)}\rho_0(\theta); \tag{A 5}$$

u_r and u_θ are calculated with (2.2) at a sufficient order for each contour.

Now, $\vec{u} = \vec{u}_{sv} + \vec{u}_{cv}$ where sv and cv are the satellites and core vortices contributions respectively. For the sv term, (A 5) shows that the basic state (circular vortices) is sufficient. We get: $u_{\theta sv} = \frac{1}{2}\gamma_0\delta_a^2 2b$ which will be neglected hereafter with respect to the cv term. Ω is calculated when determining the shape of the satellites and is the rotation rate of the equivalent point-vortices structure (see Morikawa & Swenson) with appropriate strength. It proves to be a second-order term and is thus negligible too. We also calculate

$$u_{rsv} = -\frac{\gamma_0 r_a}{2}\frac{r_a}{r_c}\left(\frac{b}{r_c}\right)^{N-1} N\sin N\theta.$$

For the cv term, (2.2) yields

$$\vec{u}_{cv}(\rho_0(\theta')\vec{e}_r) = -\frac{\gamma}{4\pi}\int_0^{2\pi} \log[\rho_0^2(\theta') + \rho_0^2(\theta) - 2\rho_0(\theta')\rho_0(\theta)\cos(\theta' - \theta)] \times(\partial_\theta \rho_0(\theta)\vec{e}_r + \rho_0(\theta)\vec{e}_\theta)\, \mathrm{d}\theta\ .$$

For $u_{\theta cv}$ the basic state is sufficient and we obtain $u_{\theta cv} = \frac{1}{2}\gamma b$. When calculating u_{rcv}, the first-order perturbation of the boundary must be retained:

$$u_{rcv}(\theta') = -\frac{\gamma b}{4\pi}\varepsilon\int_0^{2\pi} \log(1-\cos(\theta'-\theta))(\partial_\theta h(\theta)\cos(\theta'-\theta) + h(\theta)\sin(\theta'-\theta))\mathrm{d}\theta.$$

To calculate u_{rcv}, we use the integrals

$$I_p = \int_0^{2\pi} \log(1-\cos\theta)\cos p\theta \mathrm{d}\theta = -\frac{2\pi}{p}.$$

This yields the following equation for h:

$$\varepsilon\partial_\theta h = \frac{2}{\gamma}(-\tfrac{1}{2}\gamma_0 r_a \delta_a \delta_b^{N-1} N \sin N\theta + u_{rcv}).$$

Assuming $h(\theta) = \Sigma\alpha_p \sin p\theta + \beta_p(\cos p\theta - 1)$ and solving shows that

$$h(\theta) = \alpha(\cos N\theta - 1)$$

and

$$u_{rcv} = -\tfrac{1}{2}\alpha\gamma\varepsilon \sin N\theta.$$

We then get

$$\alpha = \frac{\gamma_0 r_a^2}{b(\gamma - \gamma/N)}$$

and

$$\varepsilon = \delta_b^N.$$

Using this procedure we list below the various coefficients in the perturbation expansions (6),(7),(8). The correction to the point-multipole angular velocity is

$$\omega_0 = \frac{k_1(N-1)/2 - 2\delta(N;2,3)k_0\,\delta_b^{N+1}(\gamma b/\gamma_0 r_a)}{(\gamma b^2/\gamma_0 r_a^2) + (N-1)/2},$$

where $\delta(N;2,3) = 1$ if $N = 2$ or $N = 3$ and $\delta(N;2,3) = 0$ otherwise. The various constants are

$$k_0 = \frac{\gamma_0 r_a^2}{b^2\gamma(1-1/N)},$$

$$k_1 = \sigma - \frac{2\gamma b^2}{\gamma_0 r_a^2},$$

$$k_2 = \frac{2\gamma b^2}{\gamma_0 r_a^2} - (N-1)(N-3)/4,$$

$$\mu = 3k_1\sigma/4 + k_1(N-1) + k_1\frac{\gamma b^2}{\gamma_0 r_a^2} + \delta(N;2)\left(\frac{\gamma b}{\gamma_0 r_a}\right)^4,$$

$$\nu = 2/3(N - 1 + 3\sigma - \Sigma) - 7k_1^2/6 - \frac{k_1\sigma}{3} + \frac{8\gamma b^2}{3\gamma_0 r_a^2}.$$

The sums σ and Σ are

$$\sigma = \sum_{k=1}^{N-1} \frac{\cos(k(2\pi/N))}{1-\cos(k(2\pi/N))} = (N-1)(N-5)/6,$$

$$\Sigma = \sum_{k=1}^{N-1} \frac{\cos(k(2\pi/N))}{[1-\cos(k(2\pi/N))]^2} = (N^2-1)(N^2-19)/180,$$

comparable to Dritschel's (1985) results.

Appendix B. Integral constraints

Here we derive the explicit forms of the angular momentum and area for a circular vortex and for the multipoles.

B.1. *Energy conservation*

As our model is barotropic, the energy is purely kinetic; an integration by parts using periodic boundary conditions yields the usual quantity called excess energy:

$$E = \int\int -\zeta\psi r \mathrm{d}r\mathrm{d}\theta.$$

The energy can be computed only by assuming that ζ is piecewise-constant and using the point-vortex form for ψ. This does not yield sufficient precision in the end. We will therefore not use this conservation law.

B.2. *Momentum conservation*

A similar integration by parts yields an excess angular momentum:

$$A_o = \int\int r^2\zeta r \mathrm{d}r\mathrm{d}\theta.$$

After a little algebra we get, for the multipole, the contribution of the core vortex:

$$A_{cv} = \frac{\pi\gamma b^4}{2}(1-4k_o\delta_b^N)$$

and of the satellites

$$A_{sat} = N\pi\gamma_0\frac{r_a^2 r_c^2}{2}[2+(2k_1+1)\delta_a^2+(\mu+\tfrac{1}{4}\nu+k_2+2k_1)\delta_a^4].$$

For the three-contour Rankine vortex, we remember that there is an outward motion of the peripheral vorticity in the transformation into a multipole. We therefore consider a monopole of the following form:

$$\zeta = \gamma,\ 0 \leqslant r \leqslant B;$$
$$\zeta = 0,\ B \leqslant r \leqslant A_1;$$
$$\zeta = \gamma_0,\ A_1 \leqslant r \leqslant A_2;$$
$$\zeta = 0,\ r \geqslant A_2.$$

We then get the following formula for the momentum:

$$A_o^{Rk3} = \pi\gamma\frac{B^4}{2} + \pi\gamma_0\frac{A_2^4 - A_1^4}{2}.$$

B.3. *Area conservation*

As vorticity is piecewise constant, vorticity and enstrophy conservation are equivalent to area conservation. Areas can also be easily calculated using our perturbation expansions (9) and (10):

$$A_{cv} = \pi b^2 \left(1 - 2k_o \delta_b^N\right),$$
$$A_{sat} = N\pi r_a^2 \left(1 + k_1 \delta_a^2 + \left(\tfrac{1}{2}\mu + \tfrac{1}{8}\nu + \tfrac{3}{8}k_1^2\right)\delta_a^4\right).$$

B.4. *Results*

The radii r_a, r_c, b of the multipole are given in the text (§ 6.1) with respect to A_1, A_2, B. We expand here the expressions for α_j used in the formulae.

If $N \geqslant 3$, the values of α_j are

$$\alpha_1 = \tfrac{11}{16}k_{1o}^2 - \tfrac{1}{2}k_{1o} + \frac{\gamma B^2}{\gamma_o r_A^2}k_{1o} - \tfrac{\mu}{2} - \tfrac{\nu}{8},$$
$$\alpha_2 = -\tfrac{1}{2},$$
$$\alpha_3 = -\tfrac{1}{4}k_{2o} + \tfrac{1}{2}k_{1o} + \tfrac{5}{16}k_{1o}^2.$$

If $N = 2$, the previous formulae are still correct but we must replace $(\gamma B^2/\gamma_o r_A^2)k_{1o}$ by $(\gamma B^2/\gamma_o r_A^2)(k_{1o} + 2k_{2o}B^2/r_A^2)$.

The explicit values of k_1, k_2, μ, ν are detailed in Appendix A. The subscript o in k_1 and k_2 means that these quantities, which depend on r_a and r_c, must be evaluated at r_A and r_C.

REFERENCES

ACTON, E. & DHANAK, M. R. 1993 The motion and stability of a vortex array above a pulsed surface. *J. Fluid Mech.* **247**, 231–246.

BELL, G. I. 1990 The nonlinear evolution of a perturbed axisymmetric eddy. *Woods Hole GFD Summer School Reports.* Woods Hole Oceanography Institution.

CARNEVALE, G. F. & KLOOSTERZIEL, R. C. 1994 Emergence and evolution of triangular vortices. *J. Fluid Mech.* **259**, 305–331.

CARTON, X. J., FLIERL, G. R. & POLVANI, L. M. 1989 The generation of tripoles from unstable axisymmetric isolated vortex structures. *Europhys. Lett.* **9**, 339–344.

CARTON, X. J. & MCWILLIAMS J. C. 1989 Barotropic and baroclinic instabilities of axisymmetric vortices in a quasi-geostrophic model. In *Mesoscale/Synoptic Coherent Structures in Geophysical Turbulence* (ed. J. C. J. Nihoul & B. M. Jamart), Vol.50. Elsevier.

CARTON, X. J. 1992 On the merger of shielded vortices. *Europhys. Lett.* **18**, 697–703.

CARTON, X. J. & LEGRAS B. 1994 The life-cycle of tripoles in two-dimensional incompressible flows. *J. Fluid Mech.* **267**, 53–82.

DRITSCHEL, D. G. 1985 The stability and energetics of corotating uniform vortices. *J. Fluid Mech.* **157**, 95–134.

DRITSCHEL, D. G. 1986 The nonlinear evolution of rotating configurations of uniform vorticity. *J. Fluid Mech.* **172**, 157–182.

DRITSCHEL, D. G. 1988 Contour surgery: a topological reconnection scheme for extended integrations using contour dynamics. *J. Comput. Phys.* **10**, 77.

DRITSCHEL, D. G. 1989 The stabilisation of a two-dimensional vortex strip by an adverse shear. *J. Fluid Mech.* **206**, 193–221.

FLIERL, G. R. 1988 On the instability of geostrophic vortices. *J. Fluid Mech.* **197**, 349–388.

GENT, P. R. & MCWILLIAMS, J. C. 1986 The instability of barotropic circular vortices. *Geophys. Astrophys. Fluid Dyn.* **35**, 209–233.

HEIJST, G. J. F. VAN & FLOR, J. B. 1989 Laboratory experiments on dipole structures in a stratified fluid. In *Mesoscale/Synoptic Coherent Structures in Geophysical Turbulence* (ed. J. C. J. Nihoul & B. M. Jamart), Vol. 50. Elsevier.

HEIJST, G. J. F. VAN, KLOOSTERZIEL R. C. & WILLIAMS C. W. M. 1989 Laboratory experiments on the tripolar vortices in a rotating fluid. *J. Fluid Mech.* **225**, 301–331.

HESTHAVEN, J. S., LYNOV, J. P., RASMUSSEN, J. J. & SUTYRIN G. G. 1992 Generation of tripolar vortical structures on the beta-plane. Preprint.

HOPFINGER, E. J. & HEIJST, G. J. F. VAN 1993 Vortices in rotating fluids. *Ann. Rev. Fluid Mech.* **25**, 241–289.

KLOOSTERZIEL, R. C. & HEIJST, G. J. F. VAN 1989 On tripolar vortices. In *Mesoscale/Synoptic Coherent Structures in Geophysical Turbulence* (ed. J. C. J. Nihoul & B. M. Jamart), Vol. 50. Elsevier.

KOZLOV, V. F. & MAKAROV V. G. 1985 Simulation of the instability of axisymmetric vortices using the contour dynamics method. *Izv. Akad. Nauk SSSR, Mekh. Zhidk. Gaza* **1**, 33–39. (English transl., 1985: *Fluid Dyn.* **1**, 28–34.)

LEGRAS, B. & DRITSCHEL, D. G. 1993 A comparison of the contour surgery and pseudospectral methods. *J. Comput. Phys.* **104**, 287–302.

LEGRAS, B., SANTANGELO, P. & BENZI, R. 1988 High-resolution numerical experiments for forced two-dimensional turbulence. *Europhys. Lett.* **5**, 37–42.

LEITH, C. E. 1981 Minimum-enstrophy vortices. *Phys. Fluids* **7**, 1388–1395.

LIN, S. J. 1992 Contour dynamics of tornado-like vortices. *J. Atmos. Sci.* **49**, 1745–1756.

MCWILLIAMS, J. C. & ZABUSKY, N. J. 1982 Interactions of isolated vortices. I: Modons colliding with modons. *Geophys. Astrophys. Fluid Dyn.* **19**, 207–227.

MCWILLIAMS, J. C. 1983 Interactions of isolated vortices. II: Modon generation by monopole collision. *Geophys. Astrophys. Fluid Dyn.* **24**, 1–22.

MCWILLIAMS, J. C. 1984 The emergence of isolated coherent vortices in the turbulent flow. *J.Fluid Mech.* **146**, 21–43.

MCWILLIAMS, J. C. 1990 The vortices of two-dimensional turbulence. *J. Fluid Mech.* **219**, 361–385.

MELANDER, M. V., ZABUSKY, N. J. & MCWILLIAMS, J. C. 1988 Symmetric vortex merger in two dimensions: causes and conditions. *J. Fluid Mech.* **195**, 303–340.

MIED, R. P., KIRWAN, A. D. JR & LINDEMANN, G. J. 1992 Rotating modons over isolated topographic features. *J. Phys. Oceanogr.* **22**, 1569–1582.

MOREL, Y. G. & CARTON, X. J. 1991 Generation and stability of multipolar vortices - a report from the EGS 16th General Assembly, session NP3. *SHOM Internal Reports*, and *Annales Geophys., Suppl. to vol.9*, C560.

MORIKAWA, G. K. & SWENSON, E. V. 1971 Interacting motion of rectilinear geostrophic vortices. *Phys. Fluids* **14**, 1058–1073.

ORLANDI, P. & HEIJST, G. J. F. VAN 1992 Numerical simulation of tripolar vortices in 2D flow. *Fluid Dyn. Res.* **9**, 179–206.

PIERREHUMBERT, R. T. 1980 A family of steady, translating vortex pairs with distributed vorticity. *J. Fluid Mech.* **99**, 129–144.

PINGREE, R. D., & LECANN B. 1992 Three anticyclonic Slope Water Oceanic eddies (SWODDIES) in the Southern Bay of Biscay in 1990. *Deep-Sea Res.* in press.

POLVANI, L. M. & CARTON, X. J. 1990 The tripole: a new coherent vortex structure of incompressible two-dimensional flows. *Geophys. Astrophys. Fluid Dyn.* **51**, 87–102.

STERN, M. E. 1974 Minimal properties of planetary eddies. *J. Mar. Res.* **33**, 1–13.

THOMSON, J. J. 1883 *A Treatise on the Motion of Vortex Rings*, pp. 94–108. Macmillan.

WU, H. M., OVERMAN II, E. A. & ZABUSKY, N. J. 1984 Steady-state solutions of the Euler equations in two dimensions: Rotating and translating V-States with limiting cases. I. Numerical algorithms and results. *J. Comput. Phys.* **53**, 42–71.